https://doi.org/10.5194/egusphere-2025-3458
Preprint. Discussion started: 26 August 2025

Mesozoic to Cenozoic bathymetric and gateway changes reduced Atlantic Ocean sensitivity to deoxygenation

[1,2]Nina M. Papadomanolaki, [3,4]Anta-Clarisse Sarr, [1]Anthony Gramoullé, [1]Marie Laugié, [5]Jean-Baptiste Ladant and [1]Yannick Donnadieu

[1]CEREGE, Aix Marseille Univ, CNRS, IRD, INRAE, France
[2]Institute of Geology and Paleontology, University of Münster, Münster, Germany
[3]Univ. Grenoble Alpes, Univ. Savoie Mont Blanc, CNRS, IRD, Univ. Gustave Eiffel, ISTerre, Grenoble, France
[4]Department of Earth Sciences, University of Oregon, Eugene, 97403 USA
[5]Laboratoire des Sciences du Climat et de l'Environnement, LSCE/IPSL, CEA-CNRS-UVSQ, Univ. Paris-Saclay, Gif-sur-Yvette, France

Corresponding authors: Nina M. Papadomanolaki (papadoma@uni-muenster.de)

Abstract. The magnitude of past deoxygenation events depended on multiple factors, likely including the background state of the ocean-atmosphere system. In this study, we investigate how restricted paleogeography and high atmospheric pCO_2 may have preconditioned the Mesozoic Atlantic Ocean, relative to the Cenozoic, to severe oxygen depletion. To do so, we simulate the background redox state for the moderate Paleocene-Eocene Thermal Maximum (PETM) with the Earth System Model IPSL-CM5A2 and compare it to the severe Cretaceous Oceanic Anoxic Event 2 (OAE2), with additional simulations illustrating the impact of the Tasman Gateway on post-PETM oxygenation. The deep Atlantic is, as expected, more oxygenated in the pre-PETM run due to lower Paleocene pCO_2 and ventilation through a deep Equatorial Atlantic Gateway. Yet, counterintuitively, simulated pre-PETM and pre-OAE2 deoxygenation at intermediate depths is remarkably similar, suggesting that increased background oxygenation was not the only limit on oxygen loss during the PETM. Instead, we propose that the deepening of the Equatorial Atlantic Gateway between OAE2 and the PETM isolated the low oxygen zone from the seafloor at intermediate depths, disrupting the positive biogeochemical feedbacks associated with reducing sediments and thus increasing the oxygen inventory's resilience against severe perturbations. Our simulations also suggest that the opening of the Tasman Gateway and Cenozoic pCO_2 evolution drove additional oxygenation through the onset of deep-water formation in the Atlantic sector of the Southern Ocean.

https://doi.org/10.5194/egusphere-2025-3458
Preprint. Discussion started: 26 August 2025

1 Introduction

Earth's history is punctuated by carbon cycle perturbations and intervals of climatic change that caused a reduction in concentrations marine dissolved oxygen ($[O_2]_{DISS}$) (hereafter referred to as deoxygenation) (Clapham and Renne, 2019; Mancini et al., 2024). A similar decreasing trend in modern marine $[O_2]_{DISS}$, in response to anthropogenic climate change, has been observed and is expected to continue the coming decades (Keeling et al., 2010; Breitburg et al., 2018; IPCC, 2021). The exact extent and intensity of future deoxygenation remains hard to constrain due to several factors. On the one hand, uncertainties regarding model performance, future forcing such as nutrient input, and the sensitivity of the marine $[O_2]_{DISS}$ reservoir limit current projections (Hofmann and Schellnhuber, 2009; Watson et al., 2017; Oschlies et al., 2018; Kwiatkowski et al., 2020; Ruvalcaba Baroni et al., 2020; Oschlies, 2021). On the other, deoxygenation may constitute a tipping element in the Earth system (Lenton et al., 2008; Lenton, 2013) and factors such as the original perturbation, biogeochemical feedbacks and the background ocean-atmosphere state (Hennekam et al., 2020; van de Velde et al., 2020; Reershemius and Planavsky, 2021; Mancini et al., 2024)
may trigger non-linear processes that can cause rapid amplification. The study of past deoxygenation events that differed in their magnitude and duration can aid us in improving our understanding of the system and thus our projections for the future.

Two of the most studied deoxygenation events of the past 100 Myr are the Late Cretaceous Oceanic Anoxic Event 2 (OAE2) (~94 Ma; (Meyers et al., 2012) (e.g. Arthur et al., 1990; Jenkyns, 2010) and the Paleocene-Eocene Thermal Maximum (PETM) (~56 Ma; Zeebe and Lourens, 2019) (e.g. Dickson et al., 2012; Sluijs et al., 2014; Papadomanolaki et al., 2022a). Both events have been linked to transient carbon emissions from e.g. volcanism (e.g. Turgeon and Creaser, 2008; Dickson et al., 2015; Du Vivier et al., 2015; Scaife et al., 2017; Jones et al., 2019) but, crucially, the extent of anoxic and sulfidic (euxinic) conditions was much greater during OAE2 (Dickson, 2017). Reconstructions based on molybdenum and uranium isotope records show that at its maximum, OAE2 anoxia (no free $[O_2]_{DISS}$) and euxinia (free sulfide, $[H_2S]$) may have covered up 15% and 10% of the seafloor, respectively (Dickson et al., 2016; 2017; Clarkson et al., 2018). In contrast for the PETM the maximum extent of anoxia/euxinia is estimated to have been no more than 2% (Dickson et al., 2014; 2017; Clarkson et al., 2021). This disparity has been attributed to differences in climatic forcings and/or paleogeography (Jenkyns, 2010).

Clapham and Renne (2019) suggest that long, large carbon releases, such as those associated with OAE2 (0.075 – 0.18 Pg C yr^{-1}, 18,000 – 46,000 Pg C; Clarkson et al., 2018; Papadomanolaki et al., 2022b), are usually associated with a stronger anoxia signal relative to more rapid emissions like those of the PETM (≥0.6 Pg C yr^{-1}, ≥3,000 Pg C; Zeebe et al., 2009; Gutjahr et al., 2017; Komar and Zeebe, 2017; Clarkson et al., 2021). The paleogeographical configuration also differed significantly between the Late Cretaceous and late Paleocene (Kocsis and Scotese, 2021; Scotese, 2021), with more restricted ocean basins and epicontinental seaways, while atmospheric pCO_2 decreased from the Late Cretaceous into the Cenozoic (Landwehrs et al., 2021; Cenozoic CO_2 Proxy Integration Project Consortium, 2023; Si et al., 2024). Modeling work has shown that geographical

https://doi.org/10.5194/egusphere-2025-3458
Preprint. Discussion started: 26 August 2025

and atmospheric pCO_2 changes throughout the Cretaceous impact deep ocean circulation, without quantifying the effect on $[O_2]_{DISS}$ (Poulsen et al., 2001; Donnadieu et al., 2016; Ladant et al., 2020). The lack of similar Cenozoic work further limits our ability to quantify the impact of pre-OAE2 and pre-PETM conditions on the events themselves.

In this study we use the IPSL-CM5A2 Earth System Model, to assess whether the documented changes in paleogeography and atmospheric pCO_2 from the Late Cretaceous to early Cenozoic had a significant impact on ocean oxygenation. Our focus lies on the Atlantic Ocean, the main deep, open ocean locus for OAE2 and PETM organic carbon burial (e.g. Takashima et al., 2006; Papadomanolaki et al., 2022a), whose geography and depth evolved considerably over the studied period (e.g. Parsons and Sclater, 1977; Pérez-Díaz and Eagles, 2017). Our simulations for the pre-OAE2 (90 Ma; 4× pre-industrial pCO_2; Laugié et al., 2021) and pre-PETM (60 Ma; 2× pre-industrial) reinforce the hypothesis that increased deep ocean ventilation promoted oxygenation into the Cenozoic. Yet, at intermediate water depths both simulations are characterized by a large Oxygen Minimum Zone (OMZ) which only intercepts the 90 Ma seafloor due to the shallower Cretaceous bathymetry. We speculate that this interaction, through redox-sensitive biogeochemical feedbacks in the sediments, may have been a key driver of severe OAE2 deoxygenation. Additional simulations, testing the impact of the Eocene opening of the Tasman Gateway (Bijl et al., 2013) under Early and Late Eocene pCO_2 reinforce the idea that Atlantic Ocean ventilation increased over the Cenozoic, making the PETM the last major anoxic event (Jenkyns, 2010).

2 Methods

2.1 Model description

Our simulations are performed with IPSL-CM5A2 (Sepulchre et al., 2019), an Earth System Model adapted for deep-time paleoclimate simulations. It is composed of five component models: LMDz5A for the atmosphere (Hourdin et al., 2013), ORCHIDEE for the land surface and vegetation (Krinner et al., 2005), NEMO_v3.6 for the ocean (Madec and The Nemo System Team, 2024) and LIM2 for sea-ice thermodynamics (Fichefet and Maqueda, 1997), and PISCESv2 for ocean biogeochemistry (Aumont et al., 2015). The resolution for the atmosphere is 3.75° in longitude by 1.9° in latitude, with 39 irregularly distributed vertical levels. The ocean component resolution is 2° by 2°, refined at 0.5° near the equator. It has 31 vertical levels with a thickness ranging from 10m near the surface to 500m in the deep ocean. Surface runoff is computed in ORCHIDEE and redirected to the nearest coastal grid, outside of the 200 largest drainage basins for which the runoff at the outlet represents the cumulative value for the entire area (Polcher et al., 1998; De Rosnay et al., 2003; d'Orgeval et al., 2008). For more detailed descriptions of the various components, we refer the reader to the corresponding publications.

The PISCESv2 model (Pelagic Interactions Scheme for Carbon and Ecosystem Studies; Aumont et al., 2015) simulates the biogeochemical cycles for carbon, oxygen and the five main limiting nutrients (phosphate, nitrate, iron, silica and ammonium). It includes a representation for diatoms and nanophytoplankton (primary producers) and two types of zooplankton. The limiting

https://doi.org/10.5194/egusphere-2025-3458
Preprint. Discussion started: 26 August 2025

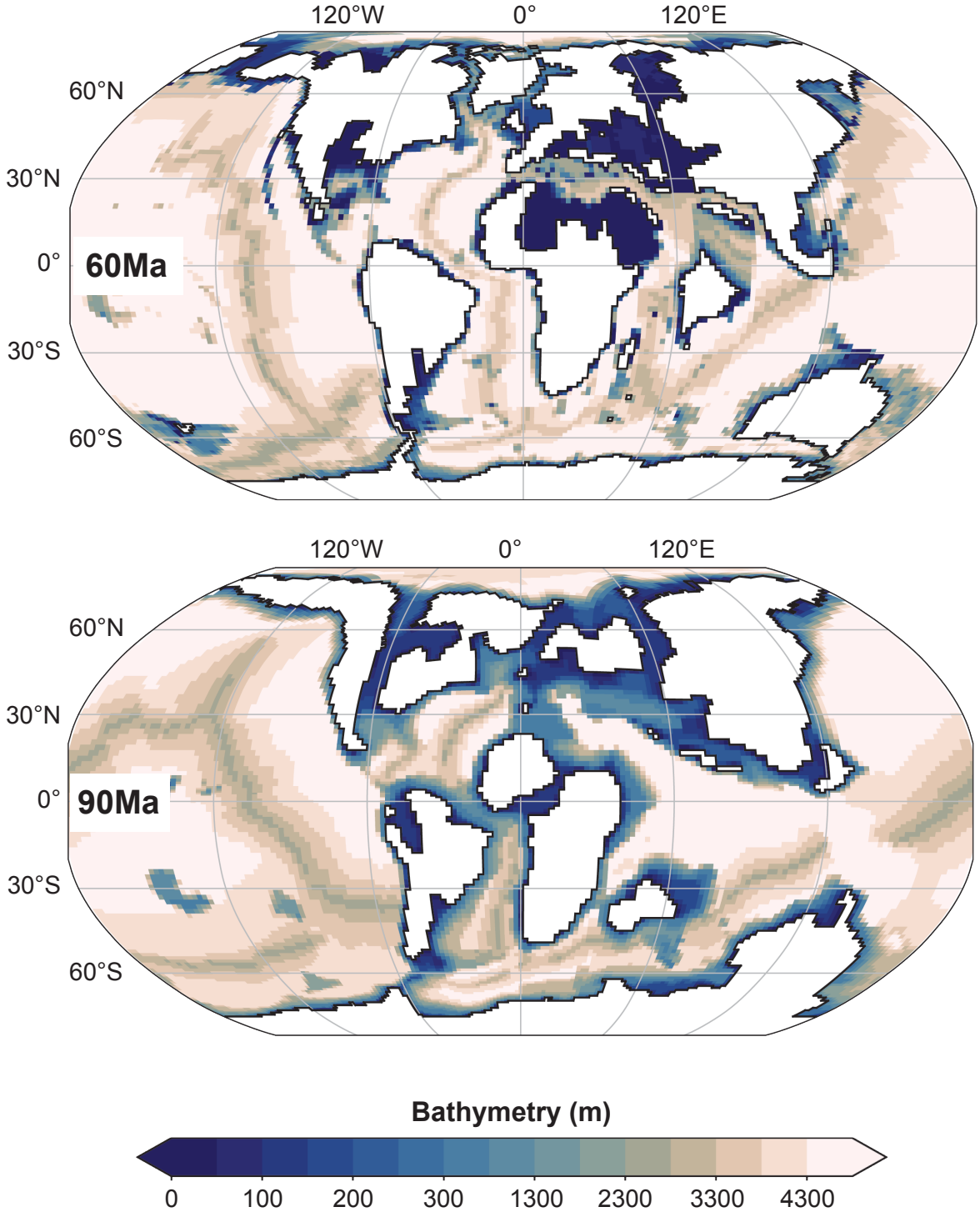

https://doi.org/10.5194/egusphere-2025-3458
Preprint. Discussion started: 26 August 2025

Figure 1. Paleogeographic configuration and bathymetry for the late Paleocene at 60Ma (left) and the Late Cretaceous at 90Ma (right).

factors for phytoplankton growth are light, nutrient availability and temperature. The C:N:P ratios of the organic pool are kept constant, whereas no ratio is imposed on the dissolved nutrient pools. Riverine and dust input, as well as the processes of denitrification and nitrogen fixation, result in variable ocean C:N:P ratios. The total global budgets are, however, kept constant at pre-industrial values. As such, the spatial distribution of dissolved nutrients is only a function of circulation and freshwater discharge, while changes in weathering have no impact.

The concentration of dissolved O_2 is a function of net primary productivity (production term), and heterotrophic respiration, oxic organic matter (OM) remineralization and nitrification (consumption terms). At the ocean surface, $[O_2]_{DISS}$ is also influenced by air-sea exchange that is dependent on temperature and salinity via the Wanninkhof (1992) parameterization. The di-oxygen concentration of the atmosphere is set to a fixed ratio of 0:21. Dissolved $[O_2]$ is split into two components (Bopp et al., 2017). The first component is $[O_2]$ saturation ($[O_2]_{SAT}$), which depends on seawater temperature and salinity. At the surface $[O_2]_{DISS}$ is close to its saturation state ($[O_2]_{DISS} \cong [O_2]_{SAT}$). The second component is Apparent $[O_2]$ Utilization (AOU) which describes the quantity of $[O_2]_{DISS}$ that has been consumed through biogeochemical processes as water masses move away from the ocean's surface. As such, AOU integrated both a biological and a ventilation signature. The three terms are linked by the following equation (Bopp et al., 2017): $[O_2]_{DISS} = [O_2]_{SAT} - AOU$.

Particulate OM in the model is represented by two pools based on the particle size (small and large) with different sinking speeds. In addition, there is a pool of semi-labile dissolved OM. The degradation of particulate to dissolved OM is a function of temperature and oxygen concentrations. Dissolved OM can be further subjected to oxic remineralization or denitrification, depending on oxygen availability. Both processes are also a function of temperature, nitrate concentrations, and bacterial activity and biomass. The fraction of particulate OM that reaches the seafloor will either be degraded through oxic remineralization or denitrification, or buried permanently. The amount of material that is buried is dependent on the flux of organic carbon to the seafloor (Dunne et al., 2007). The ratio of sedimentary oxic remineralization over denitrification is computed following Middelburg et al. (1997).

2.2 Experimental setup

Initially, we run coupled atmosphere-ocean simulations for our setups. For our baseline, pre-PETM simulation (TG_{CLOSED}) we used the Paleocene (60Ma) land-sea configuration of (Poblete et al., 2021) and their modified (Müller et al., 2008) paleo-bathymetry (**Figure 1**). In accordance with micropaleontological, tectonic and modelling reconstructions that suggest southern high-latitude gateways began opening after 49Ma (Livermore et al., 2005; Eagles et al., 2006; Bijl et al., 2013; Eagles and Jokat, 2014), we kept the Tasman Gateway and Drake Passage closed. Atmospheric CO_2 for TG_{CLOSED} was set at 2× pre-

https://doi.org/10.5194/egusphere-2025-3458
Preprint. Discussion started: 26 August 2025

industrial (560ppm), corresponding to the lower to mid-range of pCO_2 estimates prior to the PETM (Beerling and Royer, 2011; Rae et al., 2021; Cenozoic CO_2 Proxy Integration Project Consortium, 2023). Other greenhouse gases were kept at pre-industrial values, with a solar constant of 1357.5 W m^{-2} (Gough, 1981) and pre-industrial orbital configuration. The coupled simulations are followed by offline PISCES simulations as biogeochemistry typically requires a longer spin-up to equilibrium than the ocean (Séférian et al., 2016). The supply of terrestrial nutrients is calculated as the product of run-off and the riverine concentration of each relevant element. In turn, the concentrations are adjusted to conserve the global, annual amount between run-off dependent supply and the fixed modern value. The simulations do not include any variation elemental concentrations (e.g. due to different soils, vegetation, etc). Thus, any changes we simulate are due to ocean circulation and on-land precipitation.

For the comparison with the pre-OAE2 ocean, we use results from the deep Central American Seaway (CAS; ~4,000m) (*DeepCAS*) simulation by Laugié et al. (2021). This simulation was run with the same model (IPSL-CM5A2), using the Cenomanian-Turonian (90Ma) land-sea configuration of Sewall et al. (2007) with the corresponding Müller et al. (2008) paleobathymetry. Laugié et al. (2021) ran it at 4× pre-industrial (1120ppm) with a solar constant of 1353.36 W m^{-2} (Gough, 1981). Sensitivity analyses on the depth of the CAS and comparison to available proxy data indicated that this simulation best fit the pre-OAE2 distribution of oxic and anoxic conditions (Laugié et al., 2021). For the distinction different redox conditions, we use the same boundaries as Laugié et al. (2021): oxic ($[O_2]_{DISS}$>62.5 mmol m^{-3}), hypoxic (6.5<$[O_2]_{DISS}$≤62.5 mmol m^{-3}; Rabalais et al., 2010) and anoxic ($[O_2]_{DISS}$≤6.5 mmol m^{-3}). For further details, we refer the reader to the original publication.

Along with our baseline simulation, we performed two more simulations using the same 60Ma configuration (Müller et al., 2008; Poblete et al., 2021) with an open, deep Tasman Gateway for both simulations (max. depth >3000m). To mimic the progressive decline of pCO_2 from the Early Eocene onward, we ran the Early Eocene simulation at 4× pre-industrial (1120ppm; $4\times TG_{OPEN}$) and the Middle/Late Eocene at 2× pre-industrial (560ppm; TG_{OPEN}). These two setups allow us to investigate how geographical and pCO_2 changes that occurred after the PETM impacted open ocean oxygenation.

The TG_{OPEN} simulation was run for 3,600 model years with IPSL-CM5A2, the $4\times TG_{OPEN}$ simulation for 3,000 years, and TG_{CLOSED} was integrated for 2,000 years from the end state of TG_{OPEN} (**Table 1; Fig. S1**). All simulations were extended for 3,000 model years with offline PISCES simulations, forced with monthly averages of the last 100 years of the corresponding coupled simulation. Average temperature drift over the last 1000 years is <0.02°C/century (**Fig. S1**). Results are discussed using the last 100 years average climatology of each simulation.

https://doi.org/10.5194/egusphere-2025-3458
Preprint. Discussion started: 26 August 2025

Table 1. Experimental setup for the simulations presented in this study.

Simulation name	Target interval	Geography	pCO_2	Tasman Gateway	IPSL-CM5A2 coupled run duration	PISCES offline run duration	Reference
TG_{CLOSED}	Pre-PETM	60Ma	560	Closed	3,600	3,000	*This study*
$4\times TG_{OPEN}$	Early Eocene		1,120	Open	3,000		
TG_{OPEN}	Middle Eocene		560	Closed	2,000		
DeepCAS	Pre-OAE2	90Ma	1,120	Open	3,000		(Laugié et al., 2021)

2.3 Model – data comparison

Geological evidence is widely used to evaluate model outputs, especially within the Paleoclimate Modelling Intercomparison Project (PMIP; e.g. Braconnot et al., 2007; Lunt et al., 2012; Haywood et al., 2024). For the purpose of this study, it is important to assess if the spread of different redox conditions in our baseline, pre-PETM ocean is supported by proxy data. While a vast array of paleo-oxygen proxies exists, most of them are qualitative or, at best, semi-quantitative (see Hoogakker et al. (2025) for a recent review). Their interpretation is complicated by the impact of non-redox factors, the need for specific, combined proxy records, that lack of analogue environments in the modern ocean, and so forth (e.g. Tribovillard et al., 2006; Algeo and Liu, 2020; Bennett and Canfield, 2020; Hoogakker et al., 2025).

Data for the pre-PETM Atlantic Ocean is relatively scarce. In general, open ocean records indicate hypoxic rather than anoxic/euxinic conditions in the (pre-)PETM (e.g. Pälike et al., 2014; Sluijs et al., 2014; Papadomanolaki et al., 2022a), which is an additional complication as hypoxia (also dysoxia/suboxia) often denotes a range of values between fully oxic and anoxic/euxinic waters. We compiled published proxy records from the seven available Atlantic sites which reconstruct redox conditions/$[O_2]_{DISS}$ at the seafloor, during deposition. However, it is important to note that the paleodepth corresponding to these samples does not necessarily match the bathymetrical reconstruction (at model resolution) used for our simulations (Müller et al., 2008). We compare the data with $[O_2]_{DISS}$ simulated at depths equal to the paleodepth of each corresponding site.

2.3.1 Proxy interpretation

The proxies used for model output evaluation in this study are the following: (1) manganese (Mn) and uranium (U) enrichment factors (EF) (Pälike et al., 2014); (2) iodine over calcium ratios (I/Ca) (Zhou et al., 2014; 2016); (3) magnetofossils (Xue et al., 2022; 2023) and (4) molybdenum (Mo) concentrations (Papadomanolaki et al., 2022a). For the comparison with the model output we follow the interpretation of the original publication but discuss potential caveats where applicable.

https://doi.org/10.5194/egusphere-2025-3458
Preprint. Discussion started: 26 August 2025

The Mn and U EF are interpreted together as indicators of an oxygenated environment, where Mn is present as Mn oxides, or an early diagenetic, suboxic environment, where Mn represents Mn carbonates (Pälike et al., 2014). Manganese dynamics in sediments, leading to the deposition and preservation of Mn oxides or carbonates, are affected by water-column oxygenation (constant or intermittent) but also e.g. the rates of organic matter sedimentation, alkalinity and iron availability (e.g. Calvert and Pedersen, 1996; Lenz et al., 2015; Johnson et al., 2016; Dong et al., 2023). Mn carbonates can be found in sediments deposited under conditions as varying as fully oxic to periodically euxinic (e.g. Lepland and Stevens, 1998; Lyons and Severmann, 2006; Macdonald and Gobeil, 2012; Lenz et al., 2015; Lenstra et al., 2021). Currently, only qualitative interpretation of Mn and U datasets is possible, depending also on their combination with other redox proxies (Hoogakker et al., 2025).

The thermodynamically stable form of I under oxic conditions is iodate, while in anoxic deep waters and pore fluids I is predominantly present as iodide (Rue et al., 1997). When carbonates form in oxygenated settings they incorporate iodate, yet when $[O_2]_{DISS}$ is low the predominant iodide is excluded (Lu et al., 2010; Podder et al., 2017; Feng and Redfern, 2018). As a result, oxygenation favors high I/Ca values and oxygen depletion results in lower I/Ca. An additional factor is the loss of iodate in highly productive surface waters (e.g. Campos et al., 1996; 1999; Tian et al., 1996; Farrenkopf and Luther Iii, 2002; Chance et al., 2010; Bluhm et al., 2011) due to its role as a micronutrient (Küpper et al., 2011). This results in a correlation between high productivity and lower I/Ca. Calibration studies on planktic and benthic foraminiferal I/Ca have facilitated the use of this proxy across glacial-interglacial intervals (Hoogakker et al., 2018; Lu et al., 2016; Lu et al., 2020a; 2020b). In planktic foraminifera, used to reconstruct subsurface oxygenation, I/Ca values below ~2.5 µmol mol^{-1} correlate with hypoxic conditions (defined in the original publications as $[O_2]_{DISS} < \sim 70 – 100$ mmol m^{-3}) (Lu et al., 2016; Lu et al., 2020a). The I/Ca proxy can also be used to determine bottom water oxygenation when it is measured on epifaunal benthic foraminifera; the relationship, however, between benthic I/Ca and $[O_2]_{DISS}$ is not linear and low values (<~3 µmol mol^{-1}) can only indicate $[O_2]_{DISS} < \sim 50$ mmol m^{-3} (when combined with porosity data; (Lu et al., 2020b; 2021). Ongoing work on core-top calibration may improve the use of the I/Ca as a quantitative proxy (Hess et al., 2025) but for now it remains largely qualitative.

Magnetofossils (preserved biogenic magnetite/greigite) are produced motile magnetotactic bacteria that thrive in the transition zone between oxic and anoxic conditions, in the water column and in sediments (Bazylinski and Frankel, 2004; Faivre and Schuler, 2008; Kopp and Kirschvink, 2008; Lefèvre and Bazylinski, 2013). Their magnetic properties and morphology have been used extensively for environmental and redox reconstructions for the PETM, in particular because they are unaffected by carbonate dissolution (e.g. Kopp et al., 2007; Lippert and Zachos, 2007; Larrasoana et al., 2012; Chang et al., 2018; Wagner et al., 2021a; 2021b). They are purely qualitative proxies whose changing physical characteristics indicate a decrease or increase in oxygen without further constraints.

https://doi.org/10.5194/egusphere-2025-3458
Preprint. Discussion started: 26 August 2025

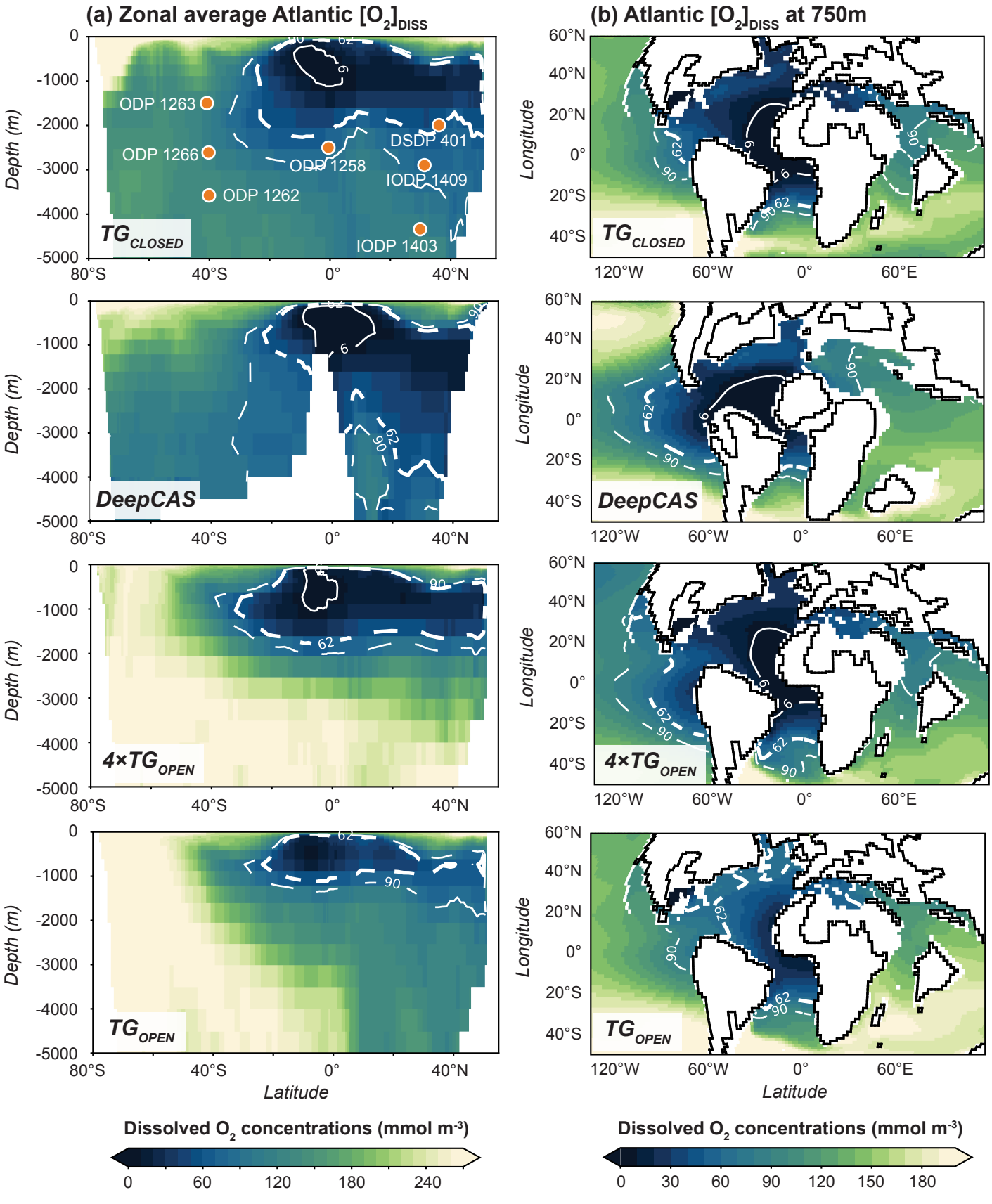

https://doi.org/10.5194/egusphere-2025-3458
Preprint. Discussion started: 26 August 2025

Figure 2. Zonally averaged oxygen concentration profiles for the Atlantic Ocean (a) and average $[O_2]_{DISS}$ in the core of the OMZ at 750m (b). *DeepCAS* results are from Laugié et al. (2021). All values in mmol m^{-3}. Solid contours: anoxia ($[O_2]_{DISS}$ < 6.5 mmol m^{-3}; $[O_2]_{DISS}$ at which denitrification starts); thick, dashed contours: hypoxia (6.5 mmol m^{-3} < $[O_2]_{DISS}$ < 62.5 mmol m^{-3}); thin, dashed contours: waters near the hypoxic threshold (62.5 mmol m^{-3} < $[O_2]_{DISS}$ < 90 mmol m^{-3}); orange symbols (a): sites used for model-data comparison (paleodepths taken from Pälike et al. (2014) and Xue et al. (2023); paleolatitudes were generated with the Paleolatitude Calculator 3.0 (Van Hinsbergen et al., 2015)).

Molybdenum is a trace-metal whose dominant form in oxic waters is the soluble molybdate (Letowski et al., 1966). The main sink for Mo is the formation of thiomolybdate under sulfidic conditions, though sequestration through e.g. adsorption to Mn oxyhydroxides is also possible (Kendall et al., 2017; Hlohowskyj et al., 2021; Hoogakker et al., 2025). Enriched authigenic Mo in sediments is generally interpreted as an indicator of a sulfidic (sedimentary) environment and can be used to distinguish between oxic to anoxic and euxinic conditions (e.g. Dickson et al., 2012; Hoogakker et al., 2025; Hardisty et al., 2018; Tribovillard et al., 2006). Basin restriction can complicate the interpretation of Mo records (Algeo and Lyons, 2006; Algeo and Tribovillard, 2009) but for the well-connected Paleocene Atlantic Ocean this is unlikely to be the case.

3 Results

3.1 Paleocene redox conditions in the Atlantic Ocean

Our 60Ma Atlantic Ocean (pre-PETM; TG_{CLOSED}) is characterized by an expansive hypoxic ($6.5<[O_2]_{DISS}\leq62.5$ mmol m^{-2}) zone with an anoxic ($[O_2]_{DISS}\leq6.5$ mmol m^{-3}) core (**Fig. 2**). This OMZ extends from the northern part of the Central Atlantic to ~35 – 20ºS in the South Atlantic, with a maximum depth of ca. 2500m (**Fig. 2**). The anoxic core is largely restricted to the Equatorial Atlantic at an average depth of 750m (**Fig. 2a**). In total, 23% of the Atlantic Ocean volume is encompassed by the OMZ; specifically, 20.2% is hypoxic and 2.8% is anoxic (**Table 2**). Only a small fraction of the low $[O_2]_{DISS}$ waters interacts with the seafloor, as 4.4% of the Atlantic seafloor is hypoxic and only 1.7% is anoxic (**Table 2**).

The waters of the Atlantic Ocean in our run are generally supersaturated with respect to $[O_2]_{DISS}$, as $[O_2]_{SAT}$ values are >300 mmol m^{-3} (**Table 3**). The low $[O_2]_{DISS}$ above 2500m and at the seafloor are a function of high AOU (**Table 3**). Deep-water formation occurs in the Southern Hemisphere (**Fig. 3a; Fig. S2**). This counterclockwise meridional overturning cell is fed by waters sinking mainly in the southern Pacific Ocean, as captured by a deep mixed layer depth (maximum values in austral winter > 1000m and 2000m; **Fig. 3b**). Aging of the deep waters en route to the Atlantic Ocean (**Fig. S3**) and a relatively weak inflow across the Tethys and CAS at intermediate depths (**Fig. 4**) contribute to the formation of the OMZ. In the highly productive Equatorial Atlantic, degradation of organic matter further increases the demand for $[O_2]_{DISS}$ (**Fig. 5a**).

https://doi.org/10.5194/egusphere-2025-3458
Preprint. Discussion started: 26 August 2025

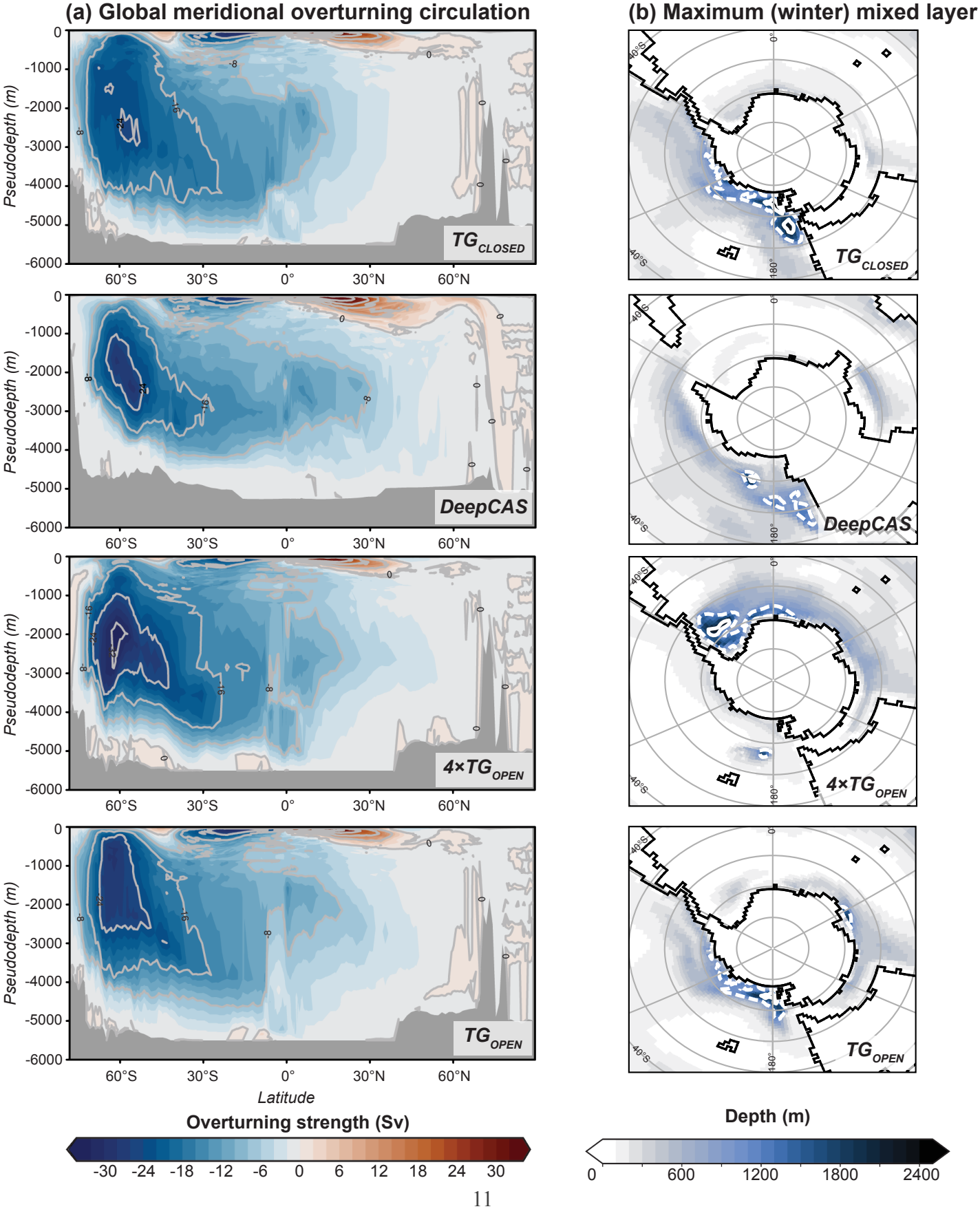

https://doi.org/10.5194/egusphere-2025-3458
Preprint. Discussion started: 26 August 2025

Figure 3. Meridional overturning circulation in Sverdrup (a) and maximum (austral winter) mixed layer depth in meters in the Southern Hemisphere (b). *DeepCAS* results from (Laugié et al., 2021). For the overturning circulation, contours are spaced at 4Sv intervals. For the mixed layer depth dashed contours indicate depths over 1000m and solid contours depths over 2000m. Note that the MOC has been computed in density coordinates and reprojected to a pseudo-depth, following de Lavergne et al. (2017).

Table 2. Percentage of the Atlantic seafloor area, and water column volume and area that is anoxic ($[O_2]_{DISS}$ <6.5 mmol m^{-3}), hypoxic (6.5 < $[O_2]_{DISS}$ < 62.5 mmol m^{-3}) or near the hypoxic threshold (62.5 < $[O_2]_{DISS}$ < 90 mmol m^{-3}). Total percentages are calculated relative to the total Atlantic seafloor area or Atlantic water column volume/area of the Atlantic Ocean. Percentages for waters shallower than 2500m are calculated relative to the seafloor area or total volume/area of the Atlantic Ocean that is shallower than 2500m. *DeepCAS* values are from (Laugié et al., 2021).

Simulation		*TG$_{CLOSED}$*		*TG$_{OPEN}$*		*4×TG$_{OPEN}$*		*DeepCAS*	
Depth (m)		<2500	Total	<2500	Total	<2500	Total	<2500	Total
Seafloor area (%)	Anoxia	7.1	1.7	4.7	1.1	8.4	2	15.5	7
	Hypoxia	17.8	4.4	9.1	2.6	15.6	3.6	32.6	24.7
	Threshold	7.1	11.7	10.8	3.3	11.5	2.9	10.1	18.7
Total volume (%)	Anoxia	4.9	2.8	1.2	0.7	5	2.9	7.7	5.4
	Hypoxia	34.6	20.2	11.3	6.5	12.2	16.2	37.3	34.2
	Threshold	15.8	17.1	14.3	8.2	11.9	6.8	7.3	12.5
Total area (%)	Anoxia	4.1	3.6	2.2	1.9	5.1	4.4	6.3	5.8
	Hypoxia	15.6	13.6	10.3	9	15.2	13.3	14	13
	Threshold	5.5	4.8	6.7	5.8	5.1	4.5	3.5	3.2
Seafloor area <2500m (%)		22.9						45.4	
Water column volume <2500m (%)		57.4						70.6	

https://doi.org/10.5194/egusphere-2025-3458
Preprint. Discussion started: 26 August 2025

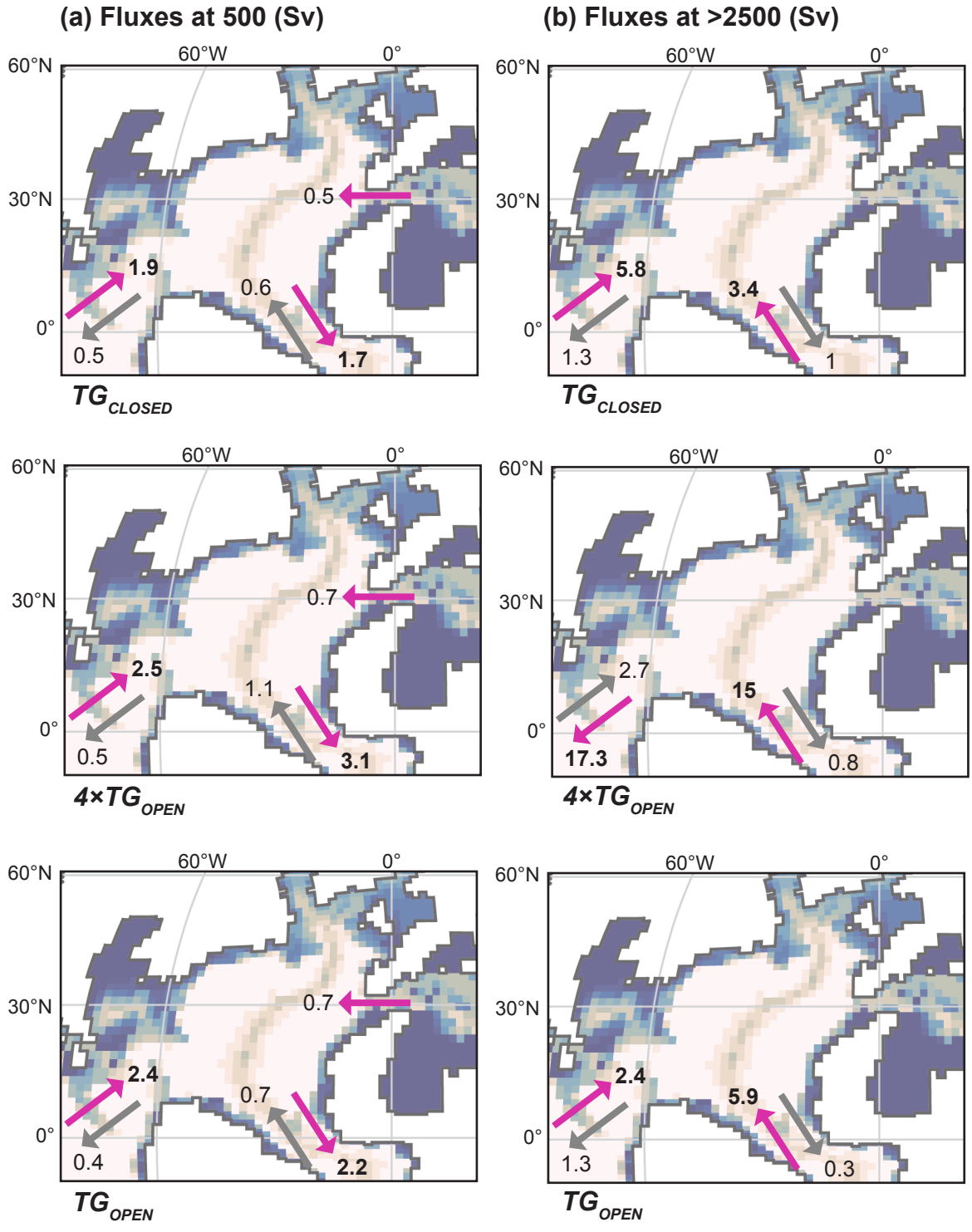

https://doi.org/10.5194/egusphere-2025-3458
Preprint. Discussion started: 26 August 2025

Figure 4. Schematic representation of the incoming and outgoing fluxes for the Central Atlantic basin across the three main gateways: values in Sverdrup are averages at 500m (a) and below 2500m (b). Bold values signify the larger flux and magenta arrows indicate the direction of the net flux across the gateway. Note that the Tethys gateway is shallow does not experience any flow in the >2500m domain.

3.2 Impact of Tasman Gateway and pCO_2 on Atlantic Ocean oxygenation

An open Tasman Gateway affects the extent of the OMZ and the ventilation of the deep ocean in our 60Ma simulations (**Fig. 6a**). At high pCO_2 (Early Eocene; *4xTG*$_{OPEN}$), the downward extent of the OMZ is reduced with hypoxia/anoxia limited to depths above ca. 2000m, and bottom water $[O_2]_{DISS}$ roughly double relative to the pre-PETM (**Fig. 2; Table 3**). Above 2000m, hypoxia is somewhat expanded laterally (**Fig. 2b**). Thus, the volume of low $[O_2]_{DISS}$ waters decreases to 20.1% while the corresponding area at the seafloor is reduced to 5.6% (**Table 2**).

The doubling in pCO_2 causes a $[O_2]_{SAT}$ reduction of 9 – 12% throughout the water column, but in the deep Atlantic this is not sufficient to counteract the decrease in AOU (**Fig. 6b, c; Table 3**). At intermediate depths, the expanded OMZ is the combined result of relatively high AOU and reduced $[O_2]_{SAT}$ (**Fig. 6b, c; Table 3**). Deep-water formation shifts from the distant southern Pacific Ocean to the Atlantic sector of the Southern Ocean (**Fig. 3**), as Southern Hemisphere westerlies shift south to push saline Indian Ocean waters into the Atlantic and Indian sectors, raising surface salinity (**Fig. S4; Table S1**). Strengthened overturning reduces deep Atlantic AOU by ca. 70% (**Fig. 6c; Table 3**). The influx across the CAS and Tethys gateway, and the outflux across the Equatorial Atlantic Gateway, all increase at intermediate depths (**Fig. 4**). In the deep Atlantic, the influx across the Equatorial Atlantic Gateway is almost tripled and the flux across the CAS is reversed into a net outflux (**Fig. 4**). Export productivity decreases along the African coast and in the northern Central Atlantic and increases are observed in parts of the Central and Southern Atlantic (**Fig. 5c**). Remineralization at the depths of the OMZ is largely equal to *TG*$_{CLOSED}$ (**Fig. 5b**).

Low pCO_2 and an open Tasman Gateway (Middle to Late Eocene; *TG*$_{OPEN}$) greatly reduce the vertical and horizontal extent of the OMZ (**Fig. 2**). The anoxic core that dominates the OMZ in the Equatorial Atlantic of the other simulation disappears completely (**Fig. 2**). Only 6.2% of the Atlantic Ocean's volume is now hypoxic/anoxic, and just 3.7% of the seafloor (**Table 2**).

https://doi.org/10.5194/egusphere-2025-3458
Preprint. Discussion started: 26 August 2025

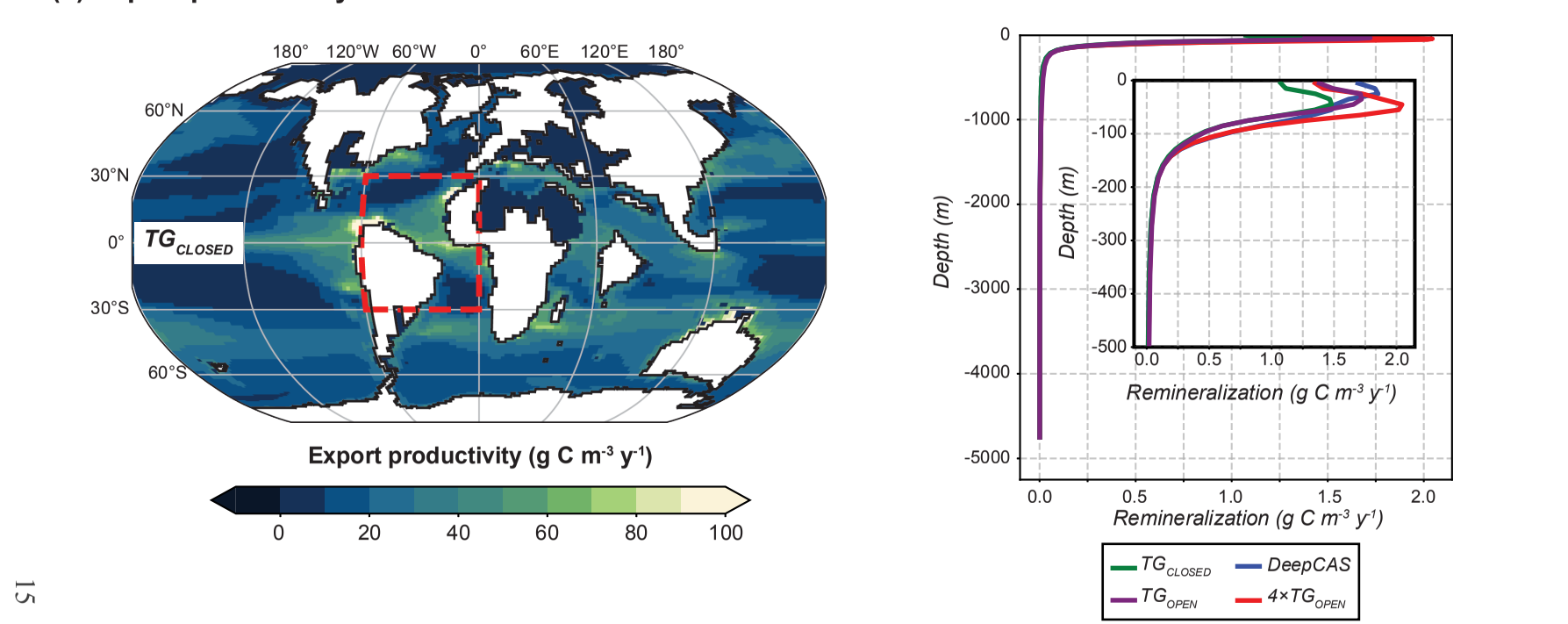

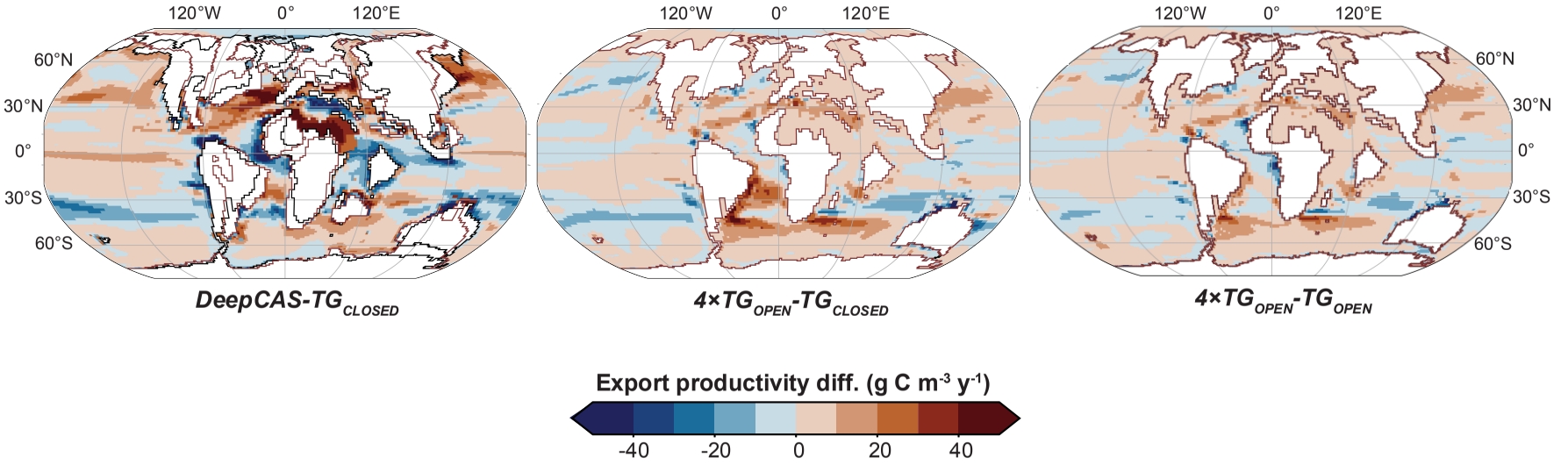

https://doi.org/10.5194/egusphere-2025-3458
Preprint. Discussion started: 26 August 2025

Figure 5. Marine export productivity across the 100m depth contour in g C m^{-3} yr^{-1} for *TG_{CLOSED}* (a) and remineralization throught the water column (surface to 500m in the inset) (b) in the high productivity region of the Equatorial Atlantic (red box in (a)). Remineralization is shown for all simulations: *TG_{CLOSED}* (green), *TG_{OPEN}* (purple), *$4{\times}TG_{OPEN}$* (red) and *DeepCAS* (blue). Bottom row Difference in export productivity at 100m (c) between (left to right) *TG_{OPEN}* and *DeepCAS*, *$4{\times}TG_{OPEN}$ and TG_{CLOSED}*, and *$4{\times}TG_{OPEN}$ and TG_{OPEN}*. *DeepCAS* results from (Laugié et al., 2021).

Oxygen saturation levels are roughly equal to the pre-PETM, and within the OMZ AOU similar to *$4xTG_{OPEN}$* (**Fig. 6b; Table 3**). In the deep ocean, AOU does not change much in the South Atlantic, yet in the Central Atlantic it is significantly increased relative to *$4xTG_{OPEN}$* (**Fig. 6c; Table 3**). Unlike *$4xTG_{OPEN}$*, the maximum mixed layer-depth indicates that deep-water formation is now split between the Pacific Ocean and the Southern Ocean, while overturning velocity is stronger than the pre-PETM and weaker than *$4xTG_{OPEN}$* (**Fig. 3**). The fluxes across the three major gateways do not change much at intermediate depths, but in the deep Atlantic they revert to values and directions more similar to the pre-PETM (**Fig. 4**). In the Equatorial Atlantic, export productivity is further reduced but the impact on remineralization is negligible (**Fig. 5**). The net result is increased ventilation at depth, which doesn't fully reach the Central Atlantic (**Figs. 2, 6a, c; Table 3**).

3.3 The Late Cretaceous Atlantic Ocean

In the 90Ma (pre-OAE2; *DeepCAS*) simulation of Laugié et al. (2021), above 2500m, the general pattern is similar to that of the pre-PETM. An anoxic core extends laterally from the Equatorial Atlantic and into the Central American Seaway (**Fig. 2**). Hypoxic waters are even more expanded, reaching well into the Pacific Ocean (**Fig. 2**). In the South Atlantic, the OMZ has a similar lateral, but restricted vertical, extent relative to the pre-PETM (**Figs. 2; 6a**). In the Equatorial Atlantic, the shallower seafloor of the gateway interacts with the anoxic waters just below 1000m (**Fig. 2**). The biggest difference with the pre-PETM simulation can be observed in the Central Atlantic. Here, hypoxia extends into the deep ocean below 2500m and interacts with a large section of the seafloor (**Fig. 1**; Laugié et al., 2021). Overall, 39.6% of the Atlantic volume and 25.4% of the seafloor are hypoxic/anoxic at 90Ma (**Table 2**).

At all depths, the higher pCO_2 forces a decrease in $[O_2]_{SAT}$ which in turn limits oxygenation (**Fig. 6b; Table 3**). On average, AOU in the pre-OAE2 Atlantic Ocean is similar to the pre-PETM, but within the OMZ it is decreased in *DeepCAS* (**Fig. 6c; Table 3**). Deep water formation is restricted to the South Pacific and is limited relative to the pre-PETM (**Fig. 3**). In the Central Atlantic, the intermediate flux across the CAS is reversed, but at depth the Equatorial Atlantic Gateway forms a barrier to circulation and limits ventilation (**Figs. 4; 6a, c**; Laugié et al., 2021). Large differences in export production are observed throughout the Atlantic Ocean: in the Central Atlantic and parts of the South Atlantic it is higher at 90Ma, but in the Equatorial and southern South Atlantic it is decreased relative to the pre-PETM (**Fig. 5**). These differences do not translate to large differences in remineralization, and thus $[O_2]_{DISS}$ consumption, within the OMZ (**Fig. 5**).

https://doi.org/10.5194/egusphere-2025-3458
Preprint. Discussion started: 26 August 2025

Table 3. Average $[O_2]_{DISS}$, O_2 saturation ($[O_2]_{SAT}$) and apparent $[O_2]$ utilization (AOU) in the core of the OMZ (620 – 880m), below 2500m and at the seafloor (mmol m^{-3}). Values are calculated for the Atlantic Ocean, between 50°N and 50°S to capture the OMZ. *DeepCAS* values are from (Laugié et al., 2021).

Simulation	Depth	Average		
		$[O_2]_{DISS}$	$[O_2]_{SAT}$	AOU
	750m	53.23	301.3	248.1
TG$_{CLOSED}$	>2500m	112.4	325.5	212.5
	Seafloor	123.2	314.2	191.0
	750m	72.75	299.5	226.8
TG$_{OPEN}$	>2500m	188.6	326.0	135.6
	Seafloor	183.3	313.4	130.0
	750m	39.61	273.8	234.2
4×TG$_{OPEN}$	>2500m	237.4	285.7	40.25
	Seafloor	223.8	277.4	53.64
	750m	51.67	269.6	217.9
DEEPCAS	>2500m	82.03	294.7	212.7
	Seafloor	79.08	278.7	199.6

https://doi.org/10.5194/egusphere-2025-3458
Preprint. Discussion started: 26 August 2025

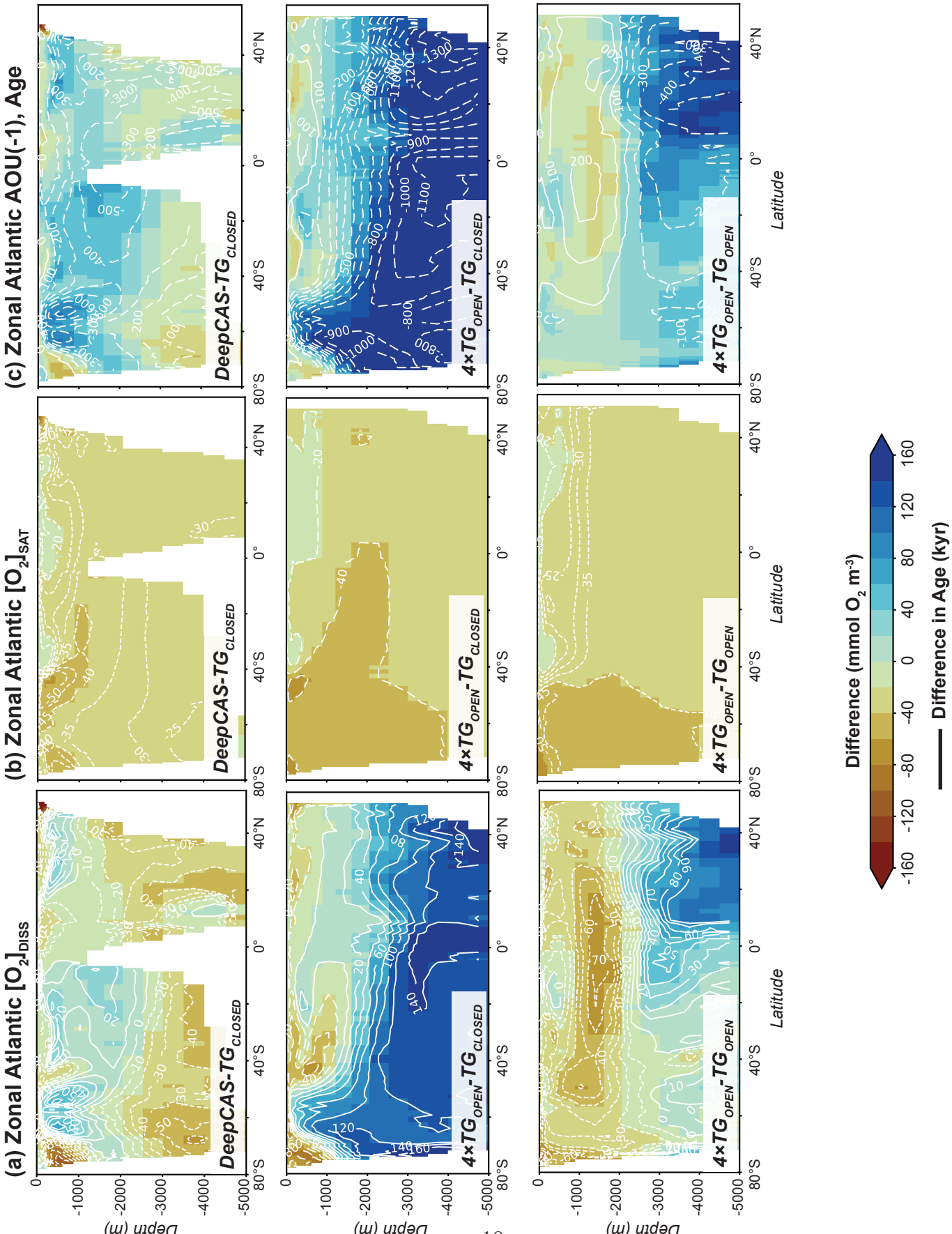

https://doi.org/10.5194/egusphere-2025-3458
Preprint. Discussion started: 26 August 2025

Figure 6. Differences in $[O_2]_{DISS}$ (a), oxygen saturation ($[O_2]_{SAT}$, b) and negative (for color scale consistency) apparent $[O_2]$ utilization (AOU; c). From left to right: *DeepCAS* minus TG_{CLOSED}, $4\times TG_{OPEN}$ minus TG_{CLOSED}, and $4\times TG_{OPEN}$ minus TG_{OPEN}. Contours in (c) mark the difference in ideal age of waters.

4 Discussion

A comparison of $[O_2]_{DISS}$, $[O_2]_{SAT}$ and AOU between the pre-PETM, pre-OAE2 and post-PETM Atlantic Ocean highlights how changes in geography and pCO_2 causes deoxygenation to expand and retract (**Fig. 2; 6**). Below, we evaluate deoxygenation in our pre-PETM simulation and discuss how the preconditioning of the Atlantic Ocean to widespread deoxygenation evolved from the Mesozoic into the Cenozoic.

4.1 Evaluation of the pre-PETM Atlantic Ocean OMZ

The presence of an $[O_2]_{DISS}$ minimum at intermediate depths of the late Paleocene/early Eocene Atlantic Ocean has been recognized by previous studies (Chun et al., 2010; Winguth et al., 2012; Pälike et al., 2014; Zhou et al., 2016). We evaluate the OMZ extent produced by IPSL-CM5A2 with the available data from six open ocean sites located in intermediate to deep waters: DSDP Site 401 (Bay of Biscay; paleodepth: 2000m); IODP Sites 1409 and 1403 (Newfoundland; paleodepth: 2913m and 4374m, respectively); ODP Site 1258 (Demerara Rise; paleodepth: 2500m); ODP Sites 1263, 1266 and 1262 (Walvis Ridge; paleodepth: 1500m, 2600m and 3600m, respectively) (symbols in **Fig. 2a**; see caption for overview of references). Manganese and uranium EF from the two deepest Walvis Ridge sites indicate oxic conditions prior to the PETM, while the shallowest site (Site 1263) was likely suboxic (Chun et al., 2010; Pälike et al., 2014). Suboxic conditions are also indicated by EF values in the Bay of Biscay and at Demerara Rise (Chun et al., 2010; Pälike et al., 2014). Ratios of I/Ca in epifaunal benthic foraminifera of Site 1262 (average: 26 µmol mol^{-1}) are interpreted as indicators of oxic bottom waters (due to the great depth of the site and the Mn EF mentioned above), so that the lower values at Site 1263 (19 – 23 µmol mol^{-1}) can be interpreted as lower $[O_2]_{DISS}$ (Zhou et al., 2016). The magnetofossil records of Newfoundland show a decrease in oxygenation for the pre-PETM, starting several hundreds of thousands of years before the event itself (Xue et al., 2023), however Mo concentrations at the deepest of these sites (Site 1403) are extremely low (≤3 ppm) indicating largely oxic conditions (Papadomanolaki et al., 2022a).

The three Walvis Ridge sites are located beyond the southernmost extent of our simulated pre-PETM (TG_{CLOSED}) OMZ. For the deepest two sites (1266 and 1262) this agrees with the interpretation of the proxy data. For Site 1263, the Mn/U EF and I/Ca values could suggest that the OMZ extended further south, and its full extent is not reproduced by our setup. We note that the I/Ca values of *Cibicoides* spp. at Site 1263 are between 10 and 15 µmol mol^{-1} prior to the PETM (Zhou et al., 2016). Species of the same genus, measured by Lu et al. (2020b), only exhibit such high values when bottom water $[O_2]_{DISS}$ > 150 mmol m^{-3} (non-OMZ conditions by our definition). We acknowledge that such semi-quantitative interpretation of very old samples has several caveats, including unknown vital effects (although *C. mundulus* is present in both the Paleocene and

https://doi.org/10.5194/egusphere-2025-3458
Preprint. Discussion started: 26 August 2025

modern samples), and that best practice requires additional data such as pore size (Lu et al., 2020b). Nevertheless, we interpret the Site 1263 record as representative of a (local) $[O_2]_{DISS}$ minimum, but not fully hypoxic conditions.

In the Central and Equatorial Atlantic, Sites 401 and 1258 are located near the lower edge of the hypoxic zone, while the two Newfoundland Sites are well below the OMZ (**Fig. 2a**). The qualitative nature of the available data does not allow a direct comparison, however the presence of magnetofossils and the enrichment of Mn and U matches the simulated low $[O_2]_{DISS}$ (if not fully hypoxic, at least well below surface values) conditions of the waters in this region. The lack of any real enrichment in Mo at Site 1403 does not support a lasting extension of hypoxia/anoxia to the deepest seafloor and in general indicates non-sulfidic sediments/oxygenated bottom waters. We conclude that we simulate an OMZ that is representative of the late Paleocene, though additional data from shallower depths are required to evaluate the lowest $[O_2]_{DISS}$.

4.2 Cretaceous to Paleocene oxygen dynamics

In the pre-OAE2 (90Ma; *DeepCAS*) simulation we observe a similar OMZ above 2500m, while the deep Central Atlantic (below 2500m) is characterized by hypoxic waters that reach the seafloor (**Fig. 2a**). Three regions emerge where oxygenation is similar or distinct for the pre-OAE2 and pre-PETM simulations, due to different mechanisms: the deep South Atlantic, the deep Central Atlantic and the OMZ. In the South Atlantic, a lack of deep-water formation in the adjacent Southern Ocean sector increases AOU in both simulations to equivalent levels, while *DeepCAS* $[O_2]_{DISS}$ are lowered further due to higher pCO_2, 4 – 5°C warmer waters and a 10% reduction in $[O_2]_{SAT}$ (**Fig. 6b**). In the deep Central Atlantic, the low $[O_2]_{DISS}$ conditions observed during the pre-OAE2 and OAE2 (e.g. van Helmond et al., 2014 and references therein) are considered the result of limited deep circulation due to a shallow Equatorial Atlantic Gateway (Arthur and Natland, 1979; de Graciansky et al., 1984; Poulsen et al., 2001; Donnadieu et al., 2016; Ladant et al., 2020). The IPSL-CM5A2 simulations presented here also produce an increase in ventilation with a deeper bathymetry in the Equatorial Atlantic, but we observe that low $[O_2]_{SAT}$ in the *DeepCAS* run exerts a stronger control on deep $[O_2]_{DISS}$ (**Fig. 6b; Table 3**). Due to the distance of the deep Atlantic from the main site of deep-water formation (**Fig. 3**) and aging of waters (**Fig. 6c**), ventilation across the Equatorial Atlantic Gateway does not supply much $[O_2]_{DISS}$ in our pre-PETM run (**Fig. 2; 4**). Within the OMZ, despite low $[O_2]_{DISS}$ availability forced by high Cretaceous temperatures and low O_2Sat, TG_{CLOSED} ventilation produces a similarly low $[O_2]_{DISS}$ environment. The sinking of oxygenated surface waters in the *DeepCAS* Indian sector of the Southern Ocean (maximum mixed layer depth > 600m; **Fig. 3b**) and the higher $[O_2]_{DISS}$ of the simulated 90Ma Tethys Ocean result in the influx of waters richer in $[O_2]_{DISS}$ across the Tethys gateway, even though the incoming TG_{CLOSED} flux is not much weaker (**Fig. 4).**

At the seafloor, we simulate a much larger areal extent of hypoxia/anoxia for the pre-OAE2 (32.7%) than the pre-PETM (6.2%) (**Table 2**) and thus reproduce the pattern that redox-sensitive isotopes reconstruct for the events themselves (Owens et al., 2013; Dickson et al., 2016; Dickson, 2017; Clarkson et al., 2018; 2021; Yao et al., 2018). Across the entire Atlantic Ocean, the area of hypoxia/anoxia is surprisingly similar between the two setups (18.8% at 90Ma and 17.2% at 60Ma; **Table 2**). This

https://doi.org/10.5194/egusphere-2025-3458
Preprint. Discussion started: 26 August 2025

discrepancy holds whether we consider the entire basin or only the seafloor and water column above 2500m (OMZ; **Table 2**). Laugié et al. (2021) show that seafloor hypoxia/anoxia in *DeepCAS* can be found in the Central and Equatorial Atlantic regions. In the Central Atlantic, as we have noted above, $[O_2]_{SAT}$ and reduced ventilation allow hypoxic conditions to permeate the deep ocean and reach the seafloor well below 2500m (**Fig. 2**). In the Equatorial region, a deeper extent of reducing conditions cannot account for most of the discrepancy as they are confined to depths shallower than 2500m in both simulations (**Fig. 2**). In fact, the areal extent of seafloor hypoxia/anoxia above 2500m (48.1% at 90Ma and 24.9% at 60Ma) closely follows the fraction of the seafloor that is shallower than 2500m (45.4% for the 90Ma paleogeography and 22.9% for the 60Ma configuration) (**Table 2**). The shallow Equatorial Atlantic Gateway region of the pre-OAE2 setup accounts for this to a significant degree. Thus, relatively higher seafloor oxygenation in the pre-PETM run is also due to bathymetric evolution rather than OMZ retraction. Proxies like molybdenum isotopes cannot distinguish between such mechanisms. As different biogeochemical processes and feedbacks are active in sediments and the water column, it is vital the extent of reducing conditions is quantified for both environments.

4.3 Ocean preconditioning to deoxygenation

A larger extent of low $[O_2]_{DISS}$ waters prior to the OAE2/PETM perturbations could facilitate a greater expansion of hypoxia and anoxia during and after a perturbation, with significant implications for biota and biogeochemical processes. The extent to which a water mass must be perturbed for a switch in redox state likely depends on how close $[O_2]_{DISS}$ are to that state (e.g. (Palastanga et al., 2011; van de Velde et al., 2020). Laugié et al. (2021) note that multiple sites which transition to anoxia during OAE2 are in regions where the *DeepCAS* setup produces low $[O_2]_{DISS}$ concentrations ($[O_2]_{DISS} < 90$ mmol m^{-3}). For the Paleocene/Eocene interval, while our simulation produces an extensive area of such low $[O_2]_{DISS}$ conditions (**Fig. 2**), there is no conclusive evidence in the geological record for a large scale switch to hypoxia and/or anoxia (Chun et al., 2010; Pälike et al., 2014; Zhou et al., 2016; Papadomanolaki et al., 2022a; Xue et al., 2023). Possible explanations for the dissimilarity in response include: (1) our simulations overestimate the extent of low $[O_2]_{DISS}$ conditions in the late Paleocene; (2) the PETM perturbation itself was insufficient to force a widespread change in redox state; (3) other factors unrelated to the perturbation were not conducive to a switch in redox state. The first option requires more (quantitative) proxy data from the edges and the core of our simulated OMZ for evaluation. Future work should also test if other models reproduce a similar result to this setup, and whether the inclusion of tidal mixing in IPSL-CM5A2 significantly changes $[O_2]_{DISS}$ distribution (Ladant et al., 2024). Similarly, the configuration of low latitude gateways may favor oxygenation through strengthened influx from outside the Atlantic. In terms of the strength of the PETM perturbation itself, larger or longer-lasting increases in pCO_2 would likely be accompanied by similarly large increase in continental weathering and nutrient supply (e.g. Wieczorek et al., 2013; Dickson et al., 2015; Jenkyns et al., 2017; Pogge Von Strandmann et al., 2021; Yobo et al., 2021) and it has been shown that this forcing in particular exerts a large control on the expansion of anoxia (Watson et al., 2017; Ozaki and Tajika, 2013; Ozaki et al., 2011). Even so, the need for stronger external forcing is compatible with the hypothesis that background conditions influenced the final outcome, as the PETM forcing may have been able to cause a switch to a largely anoxic ocean under different background

https://doi.org/10.5194/egusphere-2025-3458
Preprint. Discussion started: 26 August 2025

conditions. The same is true for factors that are not affected by the perturbation, as evidenced by the role the shallow Cretaceous Equatorial Atlantic Gateway played in limiting ventilation for the deep Central Atlantic.

The presence of large OMZ at intermediate depths in both the pre-OAE2 and pre-PETM simulations, highlights another potential mechanism favoring Cretaceous expansion of anoxia. Here, it is not just the presence of widespread, $[O_2]_{DISS}$-depleted waters but their location relative to the basin's bathymetry and productivity hotspots that matters. Multiple studies have shown that redox-sensitive biogeochemical processes occurring at the seafloor can act as powerful positive feedbacks on deoxygenation with far-reaching consequences; such processes include phosphorus regeneration (e.g. Reed et al., 2011), benthic iron release (e.g. (Wallmann et al., 2022) and marine production of the greenhouse gas N_2O (e.g. Naafs et al., 2019). Phosphorus regeneration in particular appears to be a key requirement for deoxygenation on the scale of an OAE (e.g. Mort et al., 2007; Tsandev and Slomp, 2009; Ozaki et al., 2011; Palastanga et al., 2011; Beil et al., 2020). This necessitates an interaction between hypoxic/anoxic waters and shelf/slope sediments (Ozaki and Tajika, 2013), or similar environments with a significant supply of organic matter. A major difference between the pre-OAE2 simulation and our pre-PETM results is that the OMZ at 90Ma impinges on the much shallower seafloor of the Equatorial Atlantic Gateway (**Fig. 1; 2**). Importantly, the core of the OMZ and this shallow seafloor are overlain by the highly productive Equatorial Atlantic waters (**Fig. 5**; Laugié et al., 2021) and previous work has found evidence for highly reducing conditions in this region, prior to the onset of the PETM (Kuypers et al., 2002; van Bentum et al., 2009; van Helmond et al., 2014). We hypothesize that phosphorus regeneration from these equatorial sediments, possibly combined with other biogeochemical feedbacks, resulted in a sufficiently perturbed pre-OAE2 phosphorus cycle that was primed to respond strongly to changes in nutrient input and productivity.

The simulations presented here suggest that the interaction between low $[O_2]_{DISS}$ waters and relatively shallow sediments underlying productive waters was shut down between OAE2 and the PETM, not by a dramatic shoaling and/or weakening of the OMZ, but by the progressive deepening of the Equatorial Atlantic Gateway to depths below 1000-1500m, from the Late Cretaceous onward (Channell et al., 1995; Pérez-Díaz and Eagles, 2017; Dummann et al., 2023). Thus the PETM recorded a much weaker expansion in reducing conditions but was, in turn, the last true global deoxygenation event of the Cenozoic (Jenkyns, 2010). Further changes in background conditions following the late Paleocene could explain the weaker nature of younger deoxygenation events. We find that the opening of the Tasman Gateway and the progressive decrease in atmospheric CO_2 result in Southern Ocean deep-water formation south of the Atlantic and Indian basins and improve overall oxygenation in the Atlantic Ocean (**Figs. 2, 3, 6**). Loss of $[O_2]_{DISS}$ in response to climatic events would still have had a larger impact on waters that were already depleted in $[O_2]_{DISS}$, similarly to OAE2 and the PETM, but, like the PETM, these waters no longer interacted with large areas of open ocean seafloor and its geochemistry. Thus, they left a limited imprint on the geological record. This Eocene trend of Atlantic oxygenation was likely aided by the opening of the Drake Passage (Farnsworth et al., 2019; Toumoulin et al., 2020) and continued by the onset of North Atlantic Deep Water formation (Vahlenkamp et al., 2018).

https://doi.org/10.5194/egusphere-2025-3458
Preprint. Discussion started: 26 August 2025

5 Conclusion and outlook

The IPSL-CM5A2 model simulates a pre-PETM (60Ma) Atlantic Ocean that is generally more oxygen enriched than it is for the pre-OAE2 (90Ma). Importantly, this difference is most evident in the deep Central Atlantic (>2500m), as the intermediate ocean is dominated by an OMZ of comparable size in both runs. The increase of [O_2] saturation under lower pCO_2 and the lack of barrier to deep circulation are the main controls here on the oxygenation of the deep Atlantic in the pre-PETM run. Intermediate depth deoxygenation is sustained by relatively limited ventilation for both simulations, and lower $[O_2]_{SAT}$ for the pre-OAE2 run. We argue that the Equatorial Atlantic Gateway increased the Cretaceous Atlantic Ocean's sensitivity to $[O_2]_{DISS}$ depletion, not just by limiting deep ventilation, but by providing reducing sediments where positive geochemical feedbacks could strengthen any external forcing. Bathymetrical changes, rather than OMZ evolution, appear to have removed this mechanism by the late Paleocene and, with the later contribution of an open Tasman Gateway and pCO_2 decrease, potentially reinforced the oxygen inventory's resilience to perturbation. The stability of the ocean's redox state under different boundary conditions is a topic that requires thorough evaluation if we are to correctly predict how the modern ocean will evolve the coming hundreds to thousands of years. Future work should elaborate on the results presented here by targeting factors such as nutrient input, orbital configurations and the depth of barriers to circulation, including the Walvis Ridge – Rio Grande highs. Another significant target for biogeochemical modeling is the nonlinearity of feedback processes and whether boundary conditions for past anoxic events favored large geochemical shifts,, a possibility that has been highlighted in work by Handoh and Lenton (2003), Watson et al. (2017) and Van De Velde et al. (2020).

6. Acknowledgments

N.M.P and Y.D were granted access to the HPC resources of TGCC under the allocations 2021-A0110102212 and 2022-A0090102212 made by GENCI. N.M.P. acknowledges the support from Alexander von Humboldt Foundation through the Henriette Herz Scouting Programm. A-C.S. was supported by a grant from Labex OSUG (Investissements d'avenir – ANR10 LABX56). Y.D acknowledges the support from ANR OXYMORE (ANR-18-CE31-0020).

7. Author Contributions

N.M.P.: Conceptualization, Methodology, Formal Analysis, Investigation, Visualization, Writing – Original Draft. **A.-C.S.:** Resources, Writing – Reviewing and Editing. **A.G.:** Visualization, Writing – Reviewing and Editing. **M.L.:** Resources, Writing – Reviewing and Editing. **J.-B.L.:** Resources, Visualization, Writing – Reviewing and Editing. **Y.D.:** Methodology, Investigation, Resources, Visualization, Writing – Reviewing and Editing, Project Administration, Funding Acquisition.

https://doi.org/10.5194/egusphere-2025-3458
Preprint. Discussion started: 26 August 2025

8. Open Research

LMDZ, XIOS, NEMO and ORCHIDEE are released under the terms of the CeCILL license. OASIS-MCT is released under the terms of the Lesser GNU General Public License (LGPL). IPSL-CM5A2 source code is publicly available through (Pillot, 2022). The mod.def file provides information regarding the different revisions used, namely:

- NEMOGCM branch nemo_v3_6_STABLE revision 6665
- XIOS2 branchs/xios-2.5 revision 1763
- IOIPSL/src svn tags/v2_2_2
- LMDZ5 branches/IPSLCM5A2.1 rev 3591
- branches/publications/ORCHIDEE IPSLCM5A2.1.r5307 rev 6336
- OASIS3-MCT 2.0 branch (rev 4775 IPSL server)

We recommend that you refer to the project website: http://forge.ipsl.jussieu.fr/igcmgdoc/wiki/Doc/Config/IPSLCM5A2 for a proper installation and compilation of the environment. The authors acknowledge the use of ferret (ferret.pmel.noaa.gov/Ferret/) for analysis and graphics. The authors also acknowledge the use of Crameri (2018) color maps. All model outputs and grid files required for calculations used in this study are available as a NetCDF files in Papadomanolaki and Donnadieu (2024) at (10.5281/zenodo.10560174) and in Laugié *et al*. (2021) at (10.5281/zenodo.4915873).

9. References

Algeo, T. J. and Liu, J.: A re-assessment of elemental proxies for paleoredox analysis, Chemical Geology, 540, 119549, 2020.
Algeo, T. J. and Lyons, T. W.: Mo–total organic carbon covariation in modern anoxic marine environments: Implications for analysis of paleoredox and paleohydrographic conditions, Paleoceanography, 21, 2006.
Algeo, T. J. and Tribovillard, N.: Environmental analysis of paleoceanographic systems based on molybdenum–uranium covariation, Chemical Geology, 268, 211-225, 2009.
Arthur, M., Brumsack, H.-J., Jenkyns, H., and Schlanger, S.: Stratigraphy, geochemistry, and paleoceanography of organic carbon-rich Cretaceous sequences, Cretaceous resources, events and rhythms: background and plans for research, 75-119, 1990.
Arthur, M. A. and Natland, J. H.: Carbonaceous sediments in the North and South Atlantic: The role of salinity in stable stratification of Early Cretaceous basins, Deep drilling results in the Atlantic Ocean: continental margins and paleoenvironment, 3, 375-401, 1979.
Aumont, O., Éthé, C., Tagliabue, A., Bopp, L., and Gehlen, M.: PISCES-v2: an ocean biogeochemical model for carbon and ecosystem studies, Geoscientific Model Development Discussions, 8, 1375-1509, 2015.
Bazylinski, D. A. and Frankel, R. B.: Magnetosome formation in prokaryotes, Nature Reviews Microbiology, 2, 217-230, 2004.
Beerling, D. J. and Royer, D. L.: Convergent cenozoic CO2 history, Nature geoscience, 4, 418-420, 2011.
Beil, S., Kuhnt, W., Holbourn, A., Scholz, F., Oxmann, J., Wallmann, K., Lorenzen, J., Aquit, M., and Chellai, E. H.: Cretaceous oceanic anoxic events prolonged by phosphorus cycle feedbacks, Climate of the Past, 16, 757-782, 2020.
Bennett, W. W. and Canfield, D. E.: Redox-sensitive trace metals as paleoredox proxies: A review and analysis of data from modern sediments, Earth-Science Reviews, 204, 103175, 2020.
Bijl, P. K., Bendle, J. A., Bohaty, S. M., Pross, J., Schouten, S., Tauxe, L., Stickley, C. E., McKay, R. M., Röhl, U., and Olney, M.: Eocene cooling linked to early flow across the Tasmanian Gateway, Proceedings of the National Academy of Sciences, 110, 9645-9650, 2013.

https://doi.org/10.5194/egusphere-2025-3458
Preprint. Discussion started: 26 August 2025

Bluhm, K., Croot, P., Huhn, O., Rohardt, G., and Lochte, K.: Distribution of iodide and iodate in the Atlantic sector of the southern ocean during austral summer, Deep Sea Research Part II: Topical Studies in Oceanography, 58, 2733-2748, 2011.
Bopp, L., Resplandy, L., Untersee, A., Le Mezo, P., and Kageyama, M.: Ocean (de) oxygenation from the Last Glacial Maximum to the twenty-first century: insights from Earth System models, Philosophical Transactions of the Royal Society A: Mathematical, Physical and Engineering Sciences, 375, 20160323, 2017.
Braconnot, P., Otto-Bliesner, B., Harrison, S., Joussaume, S., Peterchmitt, J.-Y., Abe-Ouchi, A., Crucifix, M., Driesschaert, E., Fichefet, T., and Hewitt, C.: Results of PMIP2 coupled simulations of the Mid-Holocene and Last Glacial Maximum–Part 1: experiments and large-scale features, Climate of the Past, 3, 261-277, 2007.
Breitburg, D., Levin, L. A., Oschlies, A., Grégoire, M., Chavez, F. P., Conley, D. J., Garçon, V., Gilbert, D., Gutiérrez, D., and Isensee, K.: Declining oxygen in the global ocean and coastal waters, Science, 359, eaam7240, 2018.
Calvert, S. E. and Pedersen, T.: Sedimentary geochemistry of manganese; implications for the environment of formation of manganiferous black shales, Economic Geology, 91, 36-47, 1996.
Campos, M., Sanders, R., and Jickells, T.: The dissolved iodate and iodide distribution in the South Atlantic from the Weddell Sea to Brazil, Marine Chemistry, 65, 167-175, 1999.
Campos, M., Farrenkopf, A., Jickells, T., and Luther Iii, G.: A comparison of dissolved iodine cycling at the Bermuda Atlantic Time-series Station and Hawaii Ocean Time-series Station, Deep Sea Research Part II: Topical Studies in Oceanography, 43, 455-466, 1996.
Cenozoic CO2 Proxy Integration Project Consortium: Toward a Cenozoic history of atmospheric CO2, Science, 382, eadi5177, 2023.
Chance, R., Weston, K., Baker, A. R., Hughes, C., Malin, G., Carpenter, L., Meredith, M. P., Clarke, A., Jickells, T. D., and Mann, P.: Seasonal and interannual variation of dissolved iodine speciation at a coastal Antarctic site, Marine Chemistry, 118, 171-181, 2010.
Chang, L., Harrison, R. J., Zeng, F., Berndt, T. A., Roberts, A. P., Heslop, D., and Zhao, X.: Coupled microbial bloom and oxygenation decline recorded by magnetofossils during the Palaeocene–Eocene Thermal Maximum, Nature Communications, 9, 4007, 2018.
Channell, J. E., Erba, E., Nakanishi, M., and Tamaki, K.: Late Jurassic-Early Cretaceous time scales and oceanic magnetic anomaly block models, 1995.
Chun, C. O., Delaney, M. L., and Zachos, J. C.: Paleoredox changes across the Paleocene-Eocene thermal maximum, Walvis Ridge (ODP Sites 1262, 1263, and 1266): Evidence from Mn and U enrichment factors, Paleoceanography, 25, 2010.
Clapham, M. E. and Renne, P. R.: Flood basalts and mass extinctions, Annual Review of Earth and Planetary Sciences, 47, 275-303, 2019.
Clarkson, M. O., Lenton, T. M., Andersen, M. B., Bagard, M.-L., Dickson, A. J., and Vance, D.: Upper limits on the extent of seafloor anoxia during the PETM from uranium isotopes, Nature Communications, 12, 399, 2021.
Clarkson, M. O., Stirling, C. H., Jenkyns, H. C., Dickson, A. J., Porcelli, D., Moy, C. M., Pogge von Strandmann, P. A., Cooke, I. R., and Lenton, T. M.: Uranium isotope evidence for two episodes of deoxygenation during Oceanic Anoxic Event 2, Proceedings of the National Academy of Sciences, 115, 2918-2923, 2018.
d'Orgeval, T., Polcher, J., and De Rosnay, P.: Sensitivity of the West African hydrological cycle in ORCHIDEE to infiltration processes, Hydrology and Earth System Sciences, 12, 1387-1401, 2008.
de Graciansky, P. d., Deroo, G., Herbin, J., Montadert, L., Müller, C., Schaaf, A., and Sigal, J.: Ocean-wide stagnation episode in the late Cretaceous, Nature, 308, 346-349, 1984.
de Lavergne, C., Madec, G., Roquet, F., Holmes, R., and Mcdougall, T. J.: Abyssal ocean overturning shaped by seafloor distribution, Nature, 551, 181-186, 2017.
De Rosnay, P., Polcher, J., Laval, K., and Sabre, M.: Integrated parameterization of irrigation in the land surface model ORCHIDEE. Validation over Indian Peninsula, Geophysical Research Letters, 30, 2003.
Dickson, A. J.: A molybdenum-isotope perspective on Phanerozoic deoxygenation events, Nature Geoscience, 10, 721-726, 2017.
Dickson, A. J., Cohen, A. S., and Coe, A. L.: Seawater oxygenation during the Paleocene-Eocene thermal maximum, Geology, 40, 639-642, 2012.
Dickson, A. J., Cohen, A. S., and Coe, A. L.: Continental margin molybdenum isotope signatures from the early Eocene, Earth and Planetary Science Letters, 404, 389-395, 2014.

https://doi.org/10.5194/egusphere-2025-3458
Preprint. Discussion started: 26 August 2025

Dickson, A. J., Jenkyns, H. C., Porcelli, D., van den Boorn, S., and Idiz, E.: Basin-scale controls on the molybdenum-isotope composition of seawater during Oceanic Anoxic Event 2 (Late Cretaceous), Geochimica et Cosmochimica Acta, 178, 291-306, 2016.

Dickson, A. J., Cohen, A. S., Coe, A. L., Davies, M., Shcherbinina, E. A., and Gavrilov, Y. O.: Evidence for weathering and volcanism during the PETM from Arctic Ocean and Peri-Tethys osmium isotope records, Palaeogeography, Palaeoclimatology, Palaeoecology, 438, 300-307, 2015.

Dong, Z.-G., Peng, Z.-D., Robbins, L. J., Konhauser, K. O., Zhang, B.-L., Zhang, L.-C., Li, J., Li, W.-J., Zhang, L., and Wang, C.-L.: Episodic ventilation of euxinic bottom waters triggers the formation of black shale-hosted Mn carbonate deposits, Geochimica et Cosmochimica Acta, 341, 17, 2023.

Donnadieu, Y., Pucéat, E., Moiroud, M., Guillocheau, F., and Deconinck, J.-F.: A better-ventilated ocean triggered by Late Cretaceous changes in continental configuration, Nature Communications, 7, 10316, 2016.

Du Vivier, A., Selby, D., Condon, D., Takashima, R., and Nishi, H.: Pacific 187Os/188Os isotope chemistry and U–Pb geochronology: Synchroneity of global Os isotope change across OAE 2, Earth and Planetary Science Letters, 428, 204-216, 2015.

Dummann, W., Hofmann, P., Herrle, J. O., Frank, M., and Wagner, T.: The early opening of the Equatorial Atlantic gateway and the evolution of Cretaceous peak warming, Geology, 51, 476-480, 2023.

Dunne, J. P., Sarmiento, J. L., and Gnanadesikan, A.: A synthesis of global particle export from the surface ocean and cycling through the ocean interior and on the seafloor, Global Biogeochemical Cycles, 21, 2007.

Eagles, G. and Jokat, W.: Tectonic reconstructions for paleobathymetry in Drake Passage, Tectonophysics, 611, 28-50, 2014.

Eagles, G., Livermore, R., and Morris, P.: Small basins in the Scotia Sea: the Eocene Drake passage gateway, Earth and Planetary Science Letters, 242, 343-353, 2006.

Faivre, D. and Schuler, D.: Magnetotactic bacteria and magnetosomes, Chemical reviews, 108, 4875-4898, 2008.

Farnsworth, A., Lunt, D., O'Brien, C., Foster, G., Inglis, G., Markwick, P., Pancost, R., and Robinson, S. A.: Climate sensitivity on geological timescales controlled by nonlinear feedbacks and ocean circulation, Geophysical Research Letters, 46, 9880-9889, 2019.

Farrenkopf, A. M. and Luther Iii, G. W.: Iodine chemistry reflects productivity and denitrification in the Arabian Sea: evidence for flux of dissolved species from sediments of western India into the OMZ, Deep Sea Research Part II: Topical Studies in Oceanography, 49, 2303-2318, 2002.

Feng, X. and Redfern, S. A.: Iodate in calcite, aragonite and vaterite CaCO3: Insights from first-principles calculations and implications for the I/Ca geochemical proxy, Geochimica et Cosmochimica Acta, 236, 351-360, 2018.

Fichefet, T. and Maqueda, M. M.: Sensitivity of a global sea ice model to the treatment of ice thermodynamics and dynamics, Journal of Geophysical Research: Oceans, 102, 12609-12646, 1997.

Gough, D.: Solar interior structure and luminosity variations, Physics of Solar Variations: Proceedings of the 14th ESLAB Symposium held in Scheveningen, The Netherlands, 16–19 September, 1980, 21-34,

Gutjahr, M., Ridgwell, A., Sexton, P. F., Anagnostou, E., Pearson, P. N., Pälike, H., Norris, R. D., Thomas, E., and Foster, G. L.: Very large release of mostly volcanic carbon during the Palaeocene–Eocene Thermal Maximum, Nature, 548, 573-577, 2017.

Handoh, I. C. and Lenton, T. M.: Periodic mid-Cretaceous oceanic anoxic events linked by oscillations of the phosphorus and oxygen biogeochemical cycles, Global Biogeochemical Cycles, 17, 2003.

Hardisty, D. S., Lyons, T. W., Riedinger, N., Isson, T. T., Owens, J. D., Aller, R. C., Rye, D. M., Planavsky, N. J., Reinhard, C. T., and Gill, B. C.: An evaluation of sedimentary molybdenum and iron as proxies for pore fluid paleoredox conditions, American Journal of Science, 318, 527-556, 2018.

Haywood, A. M., Tindall, J. C., Burton, L., Chandler, M., Dolan, A. M., Dowsett, H. J., Feng, R., Fletcher, T., Foley, K. M., and Hill, D.: Pliocene model Intercomparison project phase 3 (PlioMIP3)–Science plan and experimental design, Global and Planetary Change, 232, 104316, 2024.

Hennekam, R., van der Bolt, B., van Nes, E. H., de Lange, G. J., Scheffer, M., and Reichart, G. J.: Early-warning signals for marine anoxic events, Geophysical Research Letters, 47, e2020GL089183, 2020.

Hess, A. V., Rosenthal, Y., Zhou, X., and Bu, K.: The I/Ca paleo-oxygenation proxy in planktonic foraminifera: A multispecies core-top calibration, Geochimica et Cosmochimica Acta, 2025.

https://doi.org/10.5194/egusphere-2025-3458
Preprint. Discussion started: 26 August 2025

Hlohowskyj, S. R., Chappaz, A., and Dickson, A. J.: Molybdenum as a paleoredox proxy: Past, present, and future, Cambridge University Press2021.
Hofmann, M. and Schellnhuber, H.-J.: Oceanic acidification affects marine carbon pump and triggers extended marine oxygen holes, Proceedings of the National Academy of Sciences, 106, 3017-3022, 2009.
Hoogakker, B. A., Lu, Z., Umling, N., Jones, L., Zhou, X., Rickaby, R. E., Thunell, R., Cartapanis, O., and Galbraith, E.: Glacial expansion of oxygen-depleted seawater in the eastern tropical Pacific, Nature, 562, 410-413, 2018.
Hoogakker, B. A., Davis, C., Wang, Y., Kusch, S., Nilsson-Kerr, K., Hardisty, D. S., Jacobel, A., Reyes Macaya, D., Glock, N., and Ni, S.: Reviews and syntheses: Review of proxies for low-oxygen paleoceanographic reconstructions, Biogeosciences, 22, 863-957, 2025.
Hourdin, F., Foujols, M.-A., Codron, F., Guemas, V., Dufresne, J.-L., Bony, S., Denvil, S., Guez, L., Lott, F., and Ghattas, J.: Impact of the LMDZ atmospheric grid configuration on the climate and sensitivity of the IPSL-CM5A coupled model, Climate Dynamics, 40, 2167-2192, 2013.
IPCC: Climate Change 2021: The Physical Science Basis. Contribution of Working Group I to the Sixth Assessment Report of the Intergovernmental Panel on Climate Change, Cambridge, United Kingdom and New York, NY, USA, 2021.
Jenkyns, H. C.: Geochemistry of oceanic anoxic events, Geochemistry, Geophysics, Geosystems, 11, 2010.
Jenkyns, H. C., Dickson, A. J., Ruhl, M., and Van den Boorn, S. H.: Basalt-seawater interaction, the Plenus Cold Event, enhanced weathering and geochemical change: deconstructing Oceanic Anoxic Event 2 (Cenomanian–Turonian, Late Cretaceous), Sedimentology, 64, 16-43, 2017.
Johnson, J. E., Webb, S. M., Ma, C., and Fischer, W. W.: Manganese mineralogy and diagenesis in the sedimentary rock record, Geochimica et Cosmochimica Acta, 173, 210-231, 2016.
Jones, M. T., Percival, L. M., Stokke, E. W., Frieling, J., Mather, T. A., Riber, L., Schubert, B. A., Schultz, B., Tegner, C., and Planke, S.: Mercury anomalies across the Palaeocene–Eocene thermal maximum, Climate of the Past, 15, 217-236, 2019.
Keeling, R. F., Körtzinger, A., and Gruber, N.: Ocean deoxygenation in a warming world, Annual review of marine science, 2, 199-229, 2010.
Kendall, B., Dahl, T. W., and Anbar, A. D.: The stable isotope geochemistry of molybdenum, Reviews in Mineralogy and Geochemistry, 82, 683-732, 2017.
Komar, N. and Zeebe, R. E.: Redox-controlled carbon and phosphorus burial: A mechanism for enhanced organic carbon sequestration during the PETM, Earth and Planetary Science Letters, 479, 71-82, 2017.
Kopp, R. E. and Kirschvink, J. L.: The identification and biogeochemical interpretation of fossil magnetotactic bacteria, Earth-Science Reviews, 86, 42-61, 2008.
Kopp, R. E., Raub, T. D., Schumann, D., Vali, H., Smirnov, A. V., and Kirschvink, J. L.: Magnetofossil spike during the Paleocene-Eocene thermal maximum: Ferromagnetic resonance, rock magnetic, and electron microscopy evidence from Ancora, New Jersey, United States, Paleoceanography, 22, 2007.
Krinner, G., Viovy, N., de Noblet-Ducoudré, N., Ogée, J., Polcher, J., Friedlingstein, P., Ciais, P., Sitch, S., and Prentice, I. C.: A dynamic global vegetation model for studies of the coupled atmosphere-biosphere system, Global biogeochemical cycles, 19, 2005.
Küpper, F. C., Feiters, M. C., Olofsson, B., Kaiho, T., Yanagida, S., Zimmermann, M. B., Carpenter, L. J., Luther III, G. W., Lu, Z., and Jonsson, M.: Commemorating two centuries of iodine research: an interdisciplinary overview of current research, Angewandte Chemie International Edition, 50, 11598-11620, 2011.
Kuypers, M. M., Pancost, R. D., Nijenhuis, I. A., and Sinninghe Damsté, J. S.: Enhanced productivity led to increased organic carbon burial in the euxinic North Atlantic basin during the late Cenomanian oceanic anoxic event, Paleoceanography, 17, 3-1-3-13, 2002.
Kwiatkowski, L., Torres, O., Bopp, L., Aumont, O., Chamberlain, M., Christian, J. R., Dunne, J. P., Gehlen, M., Ilyina, T., and John, J. G.: Twenty-first century ocean warming, acidification, deoxygenation, and upper-ocean nutrient and primary production decline from CMIP6 model projections, Biogeosciences, 17, 3439-3470, 2020.
Ladant, J.-B., Poulsen, C. J., Fluteau, F., Tabor, C. R., MacLeod, K. G., Martin, E. E., Haynes, S. J., and Rostami, M. A.: Paleogeographic controls on the evolution of Late Cretaceous ocean circulation, Climate of the Past, 16, 973-1006, 2020.
Ladant, J. B., Millot-Weil, J., de Lavergne, C., Green, J. M., Nguyen, S., and Donnadieu, Y.: The role of tidal mixing in shaping Early Eocene deep ocean circulation and oxygenation, Paleoceanography and Paleoclimatology, 39, e2023PA004822, 2024.

https://doi.org/10.5194/egusphere-2025-3458
Preprint. Discussion started: 26 August 2025

Larrasoana, J. C., Roberts, A. P., Chang, L., Schellenberg, S. A., Gerald, J. D. F., Norris, R. D., and Zachos, J. C.: Magnetotactic bacterial response to Antarctic dust supply during the Palaeocene–Eocene thermal maximum, Earth and Planetary Science Letters, 333, 122-133, 2012.

Laugié, M., Donnadieu, Y., Ladant, J. B., Bopp, L., Ethé, C., and Raisson, F.: Exploring the impact of Cenomanian paleogeography and marine gateways on oceanic oxygen, Paleoceanography and Paleoclimatology, 36, e2020PA004202, 2021.

Lefèvre, C. T. and Bazylinski, D. A.: Ecology, diversity, and evolution of magnetotactic bacteria, Microbiology and Molecular Biology Reviews, 77, 497-526, 2013.

Lenstra, W., Klomp, R., Molema, F., Behrends, T., and Slomp, C.: A sequential extraction procedure for particulate manganese and its application to coastal marine sediments, Chemical Geology, 584, 120538, 2021.

Lenz, C., Jilbert, T., Conley, D., Wolthers, M., and Slomp, C.: Are recent changes in sediment manganese sequestration in the euxinic basins of the Baltic Sea linked to the expansion of hypoxia?, Biogeosciences, 12, 4875-4894, 2015.

Lepland, A. and Stevens, R. L.: Manganese authigenesis in the landsort deep, Baltic Sea, Marine geology, 151, 1-25, 1998.

Letowski, F., Serkies, J., and Niemiec, J.: Application of potential-pH diagrams for determination of the occurrence forms of trace elements in some economic mineral deposits, Economic Geology, 61, 1272-1279, 1966.

Lippert, P. C. and Zachos, J. C.: A biogenic origin for anomalous fine-grained magnetic material at the Paleocene-Eocene boundary at Wilson Lake, New Jersey, Paleoceanography, 22, 2007.

Livermore, R., Nankivell, A., Eagles, G., and Morris, P.: Paleogene opening of Drake passage, Earth and Planetary Science Letters, 236, 459-470, 2005.

Lu, W., Dickson, A. J., Thomas, E., Rickaby, R. E., Chapman, P., and Lu, Z.: Refining the planktic foraminiferal I/Ca proxy: Results from the Southeast Atlantic Ocean, Geochimica et Cosmochimica Acta, 287, 318-327, 2020a.

Lu, W., Barbosa, C. F., Rathburn, A. E., da Matta Xavier, P., Cruz, A. P., Thomas, E., Rickaby, R. E., Zhang, Y. G., and Lu, Z.: Proxies for paleo-oxygenation: A downcore comparison between benthic foraminiferal surface porosity and I/Ca, Palaeogeography, Palaeoclimatology, Palaeoecology, 579, 110588, 2021.

Lu, W., Rickaby, R. E., Hoogakker, B. A., Rathburn, A. E., Burkett, A. M., Dickson, A. J., Martínez-Méndez, G., Hillenbrand, C.-D., Zhou, X., and Thomas, E.: I/Ca in epifaunal benthic foraminifera: A semi-quantitative proxy for bottom water oxygen in a multi-proxy compilation for glacial ocean deoxygenation, Earth and Planetary Science Letters, 533, 116055, 2020b.

Lu, Z., Jenkyns, H. C., and Rickaby, R. E.: Iodine to calcium ratios in marine carbonate as a paleo-redox proxy during oceanic anoxic events, Geology, 38, 1107-1110, 2010.

Lu, Z., Hoogakker, B. A., Hillenbrand, C.-D., Zhou, X., Thomas, E., Gutchess, K. M., Lu, W., Jones, L., and Rickaby, R. E.: Oxygen depletion recorded in upper waters of the glacial Southern Ocean, Nature communications, 7, 11146, 2016.

Lunt, D. J., Dunkley Jones, T., Heinemann, M., Huber, M., LeGrande, A., Winguth, A., Loptson, C., Marotzke, J., Roberts, C., and Tindall, J.: A model–data comparison for a multi-model ensemble of early Eocene atmosphere–ocean simulations: EoMIP, Climate of the Past, 8, 1717-1736, 2012.

Lyons, T. W. and Severmann, S.: A critical look at iron paleoredox proxies: New insights from modern euxinic marine basins, Geochimica et Cosmochimica Acta, 70, 5698-5722, 2006.

Macdonald, R. W. and Gobeil, C.: Manganese sources and sinks in the Arctic Ocean with reference to periodic enrichments in basin sediments, Aquatic Geochemistry, 18, 565-591, 2012.

Madec, G. and the NEMO System Team: NEMO Ocean Engine Reference Manual, Zenodo, https://doi.org/10.5281/zenodo.1464816, 2024.

Mancini, A., Gennari, R., Lozar, F., Natalicchio, M., Della Porta, G., Bernasconi, D., Pellegrino, L., Pierre, F. D., Martire, L., and Negri, A.: Sensitivity of the thermohaline circulation during the Messinian: Toward constraining the dynamics of Mediterranean deoxygenation, Deep Sea Research Part I: Oceanographic Research Papers, 203, 104217, 2024.

Meyers, S. R., Sageman, B. B., and Arthur, M. A.: Obliquity forcing of organic matter accumulation during Oceanic Anoxic Event 2, Paleoceanography, 27, 2012.

Middelburg, J., Nieuwenhuize, J., Lubberts, R., and Van de Plassche, O.: Organic carbon isotope systematics of coastal marshes, Estuarine, Coastal and Shelf Science, 45, 681-687, 1997.

Mort, H. P., Adatte, T., Föllmi, K. B., Keller, G., Steinmann, P., Matera, V., Berner, Z., and Stüben, D.: Phosphorus and the roles of productivity and nutrient recycling during oceanic anoxic event 2, Geology, 35, 483-486, 2007.

https://doi.org/10.5194/egusphere-2025-3458
Preprint. Discussion started: 26 August 2025

Müller, R. D., Sdrolias, M., Gaina, C., and Roest, W. R.: Age, spreading rates, and spreading asymmetry of the world's ocean crust, Geochemistry, Geophysics, Geosystems, 9, 2008.
Naafs, B. D. A., Monteiro, F. M., Pearson, A., Higgins, M. B., Pancost, R. D., and Ridgwell, A.: Fundamentally different global marine nitrogen cycling in response to severe ocean deoxygenation, Proceedings of the National Academy of Sciences, 116, 24979-24984, 2019.
Oschlies, A.: A committed fourfold increase in ocean oxygen loss, Nature Communications, 12, 2307, 2021.
Oschlies, A., Brandt, P., Stramma, L., and Schmidtko, S.: Drivers and mechanisms of ocean deoxygenation, Nature geoscience, 11, 467-473, 2018.
Owens, J. D., Gill, B. C., Jenkyns, H. C., Bates, S. M., Severmann, S., Kuypers, M. M., Woodfine, R. G., and Lyons, T. W.: Sulfur isotopes track the global extent and dynamics of euxinia during Cretaceous Oceanic Anoxic Event 2, Proceedings of the National Academy of Sciences, 110, 18407-18412, 2013.
Ozaki, K. and Tajika, E.: Biogeochemical effects of atmospheric oxygen concentration, phosphorus weathering, and sea-level stand on oceanic redox chemistry: Implications for greenhouse climates, Earth and Planetary Science Letters, 373, 129-139, 2013.
Ozaki, K., Tajima, S., and Tajika, E.: Conditions required for oceanic anoxia/euxinia: Constraints from a one-dimensional ocean biogeochemical cycle model, Earth and Planetary Science Letters, 304, 270-279, 2011.
Palastanga, V., Slomp, C., and Heinze, C.: Long-term controls on ocean phosphorus and oxygen in a global biogeochemical model, Global Biogeochemical Cycles, 25, 2011.
Pälike, C., Delaney, M. L., and Zachos, J. C.: Deep-sea redox across the Paleocene-Eocene thermal maximum, Geochemistry, Geophysics, Geosystems, 15, 1038-1053, 2014.
Papadomanolaki, N. M., Sluijs, A., and Slomp, C. P.: Eutrophication and deoxygenation forcing of marginal marine organic carbon burial during the PETM, Paleoceanography and Paleoclimatology, 37, e2021PA004232, 2022a.
Papadomanolaki, N. M., Van Helmond, N. A., Pälike, H., Sluijs, A., and Slomp, C. P.: Quantifying volcanism and organic carbon burial across Oceanic Anoxic Event 2, Geology, 50, 511-515, 2022b.
Parsons, B. and Sclater, J. G.: An analysis of the variation of ocean floor bathymetry and heat flow with age, Journal of Geophysical Research, 82, 24, 1977.
Pérez-Díaz, L. and Eagles, G.: South Atlantic paleobathymetry since early Cretaceous, Scientific reports, 7, 1-16, 2017.
Poblete, F., Dupont-Nivet, G., Licht, A., Van Hinsbergen, D. J., Roperch, P., Mihalynuk, M., Johnston, S., Guillocheau, F., Baby, G., and Fluteau, F.: Towards interactive global paleogeographic maps, new reconstructions at 60, 40 and 20 Ma, Earth-Science Reviews, 214, 103508, 2021.
Podder, J., Lin, J., Sun, W., Botis, S., Tse, J., Chen, N., Hu, Y., Li, D., Seaman, J., and Pan, Y.: Iodate in calcite and vaterite: Insights from synchrotron X-ray absorption spectroscopy and first-principles calculations, Geochimica et Cosmochimica Acta, 198, 218-228, 2017.
Pogge von Strandmann, P. A., Jones, M. T., West, A. J., Murphy, M. J., Stokke, E. W., Tarbuck, G., Wilson, D. J., Pearce, C. R., and Schmidt, D. N.: Lithium isotope evidence for enhanced weathering and erosion during the Paleocene-Eocene Thermal Maximum, Science Advances, 7, eabh4224, 2021.
Polcher, J., McAvaney, B., Viterbo, P., Gaertner, M.-A., Hahmann, A., Mahfouf, J.-F., Noilhan, J., Phillips, T., Pitman, A., and Schlosser, C.: A proposal for a general interface between land surface schemes and general circulation models, Global and Planetary Change, 19, 261-276, 1998.
Poulsen, C. J., Barron, E. J., Arthur, M. A., and Peterson, W. H.: Response of the mid-Cretaceous global oceanic circulation to tectonic and CO2 forcings, Paleoceanography, 16, 576-592, 2001.
Rabalais, N., Diaz, R. J., Levin, L., Turner, R. E., Gilbert, D., and Zhang, J.: Dynamics and distribution of natural and human-caused hypoxia, Biogeosciences, 7, 585-619, 2010.
Rae, J. W., Zhang, Y. G., Liu, X., Foster, G. L., Stoll, H. M., and Whiteford, R. D.: Atmospheric CO2 over the past 66 million years from marine archives, Annual Review of Earth and Planetary Sciences, 49, 609-641, 2021.
Reed, D. C., Slomp, C. P., and Gustafsson, B. G.: Sedimentary phosphorus dynamics and the evolution of bottom-water hypoxia: A coupled benthic–pelagic model of a coastal system, Limnology and Oceanography, 56, 1075-1092, 2011.
Reershemius, T. and Planavsky, N. J.: What controls the duration and intensity of ocean anoxic events in the Paleozoic and the Mesozoic?, Earth-Science Reviews, 221, 103787, 2021.

https://doi.org/10.5194/egusphere-2025-3458
Preprint. Discussion started: 26 August 2025

Rue, E. L., Smith, G. J., Cutter, G. A., and Bruland, K. W.: The response of trace element redox couples to suboxic conditions in the water column, Deep Sea Research Part I: Oceanographic Research Papers, 44, 113-134, 1997.
Ruvalcaba Baroni, I., Palastanga, V., and Slomp, C. P.: Enhanced organic carbon burial in sediments of oxygen minimum zones upon ocean deoxygenation, Frontiers in Marine Science, 6, 839, 2020.
Scaife, J., Ruhl, M., Dickson, A., Mather, T., Jenkyns, H., Percival, L., Hesselbo, S., Cartwright, J., Eldrett, J., and Bergman, S.: Sedimentary mercury enrichments as a marker for submarine large igneous province volcanism? Evidence from the Mid-Cenomanian event and Oceanic Anoxic Event 2 (Late Cretaceous), Geochemistry, Geophysics, Geosystems, 18, 4253-4275, 2017.
Séférian, R., Gehlen, M., Bopp, L., Resplandy, L., Orr, J. C., Marti, O., Dunne, J. P., Christian, J. R., Doney, S. C., and Ilyina, T.: Inconsistent strategies to spin up models in CMIP5: Implications for ocean biogeochemical model performance assessment, Geoscientific Model Development, 9, 1827-1851, 2016.
Sepulchre, P., Caubel, A., Ladant, J.-B., Bopp, L., Boucher, O., Braconnot, P., Brockmann, P., Cozic, A., Donnadieu, Y., and Estella-Perez, V.: IPSL-CM5A2. An Earth System Model designed for multi-millennial climate simulations, Geoscientific Model Development Discussions, 2019, 1-57, 2019.
Sewall, J. v., Van De Wal, R., Van Der Zwan, K., Van Oosterhout, C., Dijkstra, H., and Scotese, C.: Climate model boundary conditions for four Cretaceous time slices, Climate of the Past, 3, 647-657, 2007.
Sluijs, A., Van Roij, L., Harrington, G., Schouten, S., Sessa, J., LeVay, L., Reichart, G.-J., and Slomp, C.: Warming, euxinia and sea level rise during the Paleocene–Eocene Thermal Maximum on the Gulf Coastal Plain: implications for ocean oxygenation and nutrient cycling, Climate of the Past, 10, 1421-1439, 2014.
Takashima, R., Nishi, H., Huber, B. T., and Leckie, R. M.: Greenhouse world and the Mesozoic ocean, Oceanography, 2006.
Tian, R., Marty, J., Nicolas, E., Chiavérini, J., Ruiz-Ping, D., and Pizay, M.: Iodine speciation: a potential indicator to evaluate new production versus regenerated production, Deep Sea Research Part I: Oceanographic Research Papers, 43, 723-738, 1996.
Toumoulin, A., Donnadieu, Y., Ladant, J. B., Batenburg, S., Poblete, F., and Dupont-Nivet, G.: Quantifying the effect of the Drake Passage opening on the Eocene Ocean, Paleoceanography and Paleoclimatology, 35, e2020PA003889, 2020.
Tribovillard, N., Algeo, T. J., Lyons, T., and Riboulleau, A.: Trace metals as paleoredox and paleoproductivity proxies: an update, Chemical geology, 232, 12-32, 2006.
Tsandev, I. and Slomp, C.: Modeling phosphorus cycling and carbon burial during Cretaceous Oceanic Anoxic Events, Earth and Planetary Science Letters, 286, 71-79, 2009.
Turgeon, S. C. and Creaser, R. A.: Cretaceous oceanic anoxic event 2 triggered by a massive magmatic episode, Nature, 454, 323-326, 2008.
Vahlenkamp, M., Niezgodzki, I., De Vleeschouwer, D., Lohmann, G., Bickert, T., and Pälike, H.: Ocean and climate response to North Atlantic seaway changes at the onset of long-term Eocene cooling, Earth and Planetary Science Letters, 498, 185-195, 2018.
van Bentum, E. C., Hetzel, A., Brumsack, H.-J., Forster, A., Reichart, G.-J., and Damsté, J. S. S.: Reconstruction of water column anoxia in the equatorial Atlantic during the Cenomanian–Turonian oceanic anoxic event using biomarker and trace metal proxies, Palaeogeography, Palaeoclimatology, Palaeoecology, 280, 489-498, 2009.
van de Velde, S. J., Reinhard, C. T., Ridgwell, A., and Meysman, F. J.: Bistability in the redox chemistry of sediments and oceans, Proceedings of the National Academy of Sciences, 117, 33043-33050, 2020.
van Helmond, N. A., Ruvalcaba Baroni, I., Sluijs, A., Sinninghe Damsté, J. S., and Slomp, C. P.: Spatial extent and degree of oxygen depletion in the deep proto-N orth A tlantic basin during O ceanic A noxic E vent 2, Geochemistry, Geophysics, Geosystems, 15, 4254-4266, 2014.
van Hinsbergen, D. J., De Groot, L. V., van Schaik, S. J., Spakman, W., Bijl, P. K., Sluijs, A., Langereis, C. G., and Brinkhuis, H.: A paleolatitude calculator for paleoclimate studies, PloS one, 10, e0126946, 2015.
Wagner, C. L., Egli, R., Lascu, I., Lippert, P. C., Livi, K. J., and Sears, H. B.: In situ magnetic identification of giant, needle-shaped magnetofossils in Paleocene–Eocene Thermal Maximum sediments, Proceedings of the National Academy of Sciences, 118, e2018169118, 2021a.
Wagner, C. L., Lascu, I., Lippert, P. C., Egli, R., Livi, K. J., and Sears, H. B.: Diversification of iron-biomineralizing organisms during the Paleocene-Eocene Thermal Maximum: Evidence from quantitative unmixing of magnetic signatures of conventional and giant magnetofossils, Paleoceanography and Paleoclimatology, 36, e2021PA004225, 2021b.

https://doi.org/10.5194/egusphere-2025-3458
Preprint. Discussion started: 26 August 2025

Wallmann, K., José, Y. S., Hopwood, M. J., Somes, C. J., Dale, A. W., Scholz, F., Achterberg, E. P., and Oschlies, A.: Biogeochemical feedbacks may amplify ongoing and future ocean deoxygenation: a case study from the Peruvian oxygen minimum zone, Biogeochemistry, 159, 45-67, 2022.

Wanninkhof, R.: Relationship between wind speed and gas exchange over the ocean, Journal of Geophysical Research: Oceans, 97, 7373-7382, 1992.

Watson, A. J., Lenton, T. M., and Mills, B. J.: Ocean deoxygenation, the global phosphorus cycle and the possibility of human-caused large-scale ocean anoxia, Philosophical Transactions of the Royal Society A: Mathematical, Physical and Engineering Sciences, 375, 20160318, 2017.

Wieczorek, R., Fantle, M. S., Kump, L. R., and Ravizza, G.: Geochemical evidence for volcanic activity prior to and enhanced terrestrial weathering during the Paleocene Eocene Thermal Maximum, Geochimica et Cosmochimica Acta, 119, 391-410, 2013.

Winguth, A. M., Thomas, E., and Winguth, C.: Global decline in ocean ventilation, oxygenation, and productivity during the Paleocene-Eocene Thermal Maximum: Implications for the benthic extinction, Geology, 40, 263-266, 2012.

Xue, P., Chang, L., and Thomas, E.: Abrupt Northwest Atlantic deep-sea oxygenation decline preceded the Palaeocene-Eocene Thermal Maximum, Earth and Planetary Science Letters, 618, 118304, 2023.

Xue, P., Chang, L., Dickens, G. R., and Thomas, E.: A depth-transect of ocean deoxygenation during the Paleocene-Eocene Thermal Maximum: Magnetofossils in sediment cores from the southeast Atlantic, Journal of Geophysical Research: Solid Earth, 127, e2022JB024714, 2022.

Yao, W., Paytan, A., and Wortmann, U. G.: Large-scale ocean deoxygenation during the Paleocene-Eocene Thermal Maximum, Science, 361, 804-806, 2018.

Yobo, L. N., Brandon, A. D., Holmden, C., Lau, K. V., and Eldrett, J.: Changing inputs of continental and submarine weathering sources of Sr to the oceans during OAE 2, Geochimica et cosmochimica acta, 303, 205-222, 2021.

Zeebe, R. E. and Lourens, L. J.: Solar System chaos and the Paleocene–Eocene boundary age constrained by geology and astronomy, Science, 365, 926-929, 2019.

Zeebe, R. E., Zachos, J. C., and Dickens, G. R.: Carbon dioxide forcing alone insufficient to explain Palaeocene–Eocene Thermal Maximum warming, Nature Geoscience, 2, 576-580, 2009.

Zhou, X., Thomas, E., Rickaby, R. E., Winguth, A. M., and Lu, Z.: I/Ca evidence for upper ocean deoxygenation during the PETM, Paleoceanography, 29, 964-975, 2014.

Zhou, X., Thomas, E., Winguth, A., Ridgwell, A., Scher, H., Hoogakker, B. A., Rickaby, R., and Lu, Z.: Expanded oxygen minimum zones during the late Paleocene-early Eocene: Hints from multiproxy comparison and ocean modeling, Paleoceanography, 31, 1532-1546, 2016.